The Peru Upwelling and the Ventilation of the South Pacific Thermocline

J. R. TOGGWEILER AND K. DIXON

NOAA Geophysical Fluid Dynamics Laboratory, Princeton University, Princeton, New Jersey

W. S. BROECKER

Lamont-Doherty Geological Observatory of Columbia University, Palisades, New York

A reconstruction of the prebomb $\Delta^{14}C$ distribution in the tropical Pacific using data from old coral heads shows that surface waters with the lowest $\Delta^{14}C$ content are found distinctly south of the equator. Prebomb, low-$\Delta^{14}C$ surface water appears to owe its origin to the upwelling of $\sim 15°C$ water off the coast of Peru. The low-$\Delta^{14}C$ water upwelling off Peru is shown to be derived from the "13° Water" thermostad (11°–14°C) of the Equatorial Undercurrent. Untritiated water in the lower part of the undercurrent had nearly the same $\Delta^{14}C$ content during the Geochemical Ocean Sections Study (GEOSECS) as the prebomb growth bands in Druffel's (1981) Galapagos coral. Similar $\Delta^{14}C$ levels were observed in 9°–10°C water in the southwest Pacific thermocline in the late 1950s. We suggest that the low-$\Delta^{14}C$ water upwelling off Peru and the thermostad water in the undercurrent both originate as $\sim 8°C$ water in the subantarctic region of the southwest Pacific. This prescription points to the "lighter variety" of Subantarctic Mode Water (7°–10°C) as a possible source. Because prebomb $\Delta^{14}C$ is so weakly forced by exchange of carbon isotopes with the atmosphere, thermocline levels of $\Delta^{14}C$ should be particularly unaffected by diapycnal mixing with warmer overlying water types. We argue that successively less dense features of the South Pacific thermocline, like the Subantarctic Mode Water, the equatorial 13°C Water, and the Peru upwelling, may be part of a single process of thermocline ventilation. Each evolves from the other by diapycnal alteration, while prebomb $\Delta^{14}C$ is nearly conserved. Detailed comparisons are made between the coral $\Delta^{14}C$ distribution and a model simulation of radiocarbon in Toggweiler et al. (1989). While the $\Delta^{14}C$ data suggest a southern hemisphere thermocline origin for the equatorial $\Delta^{14}C$ minimum, the model produces its $\Delta^{14}C$ minimum by upwelling abyssal water to the surface via the equatorial divergence. In an appendix to the paper we present a new set of coral $\Delta^{14}C$ measurements produced over the last 10 years at Lamont-Doherty Geological Observatory and compile a post-1950 set of published coral $\Delta^{14}C$ measurements for use in model validation studies.

INTRODUCTION

The dynamical basis for upwelling in the equatorial Pacific is a familiar concept to every first-year oceanography student. The trade winds blowing out of the east and the change in sign of the Coriolis force at the equator produce a strong divergence in the surface transport. Continuity requires that subsurface water be drawn up from below. A number of studies over the last decade have attempted to identify the subsurface origins of the upwelled water using dynamical methods and tracer observations [*Wyrtki*, 1981; *Quay et al.*, 1983; *Bryden and Brady*, 1985; *Fine et al.*, 1987; *Druffel*, 1987]. These studies overwhelmingly point to shallow, upper thermocline sources in the regions north and south of the equator. *Wyrtki* [1981] calculated the total volume of upwelling to be about 50×10^6 m^3 s^{-1}. He argued that the equatorial Pacific heat budget constrains the upwelled water to be about 3°C cooler than the water flowing away at the surface (i.e., generally warmer than 22°C).

The Pacific Geochemical Ocean Sections Study (GEOSECS) expedition in the early 1970s documented a wide expanse of low-$\Delta^{14}C$ surface water over the entire tropical region [*Broecker et al.*, 1985]. Low $^{14}C/^{12}C$ ratios in seawater generally characterize water masses which have been isolated from the atmosphere for a long time ($\sim$ centuries), a time scale much longer than that expected for the ventilation

of upper thermocline water warmer than 22°C. *Broecker et al.* [1985] concluded that colder, deeper water must be upwelling along the equator and spreading to the north and south. Figure 1 [from *Broecker and Peng*, 1982] summarizes the GEOSECS surface ^{14}C record in the Atlantic, Pacific, and Indian oceans. It shows that tropical surface waters in all three oceans had much lower $\Delta^{14}C$ contents than surface waters in the subtropics.

The Pacific GEOSECS cruises took place in 1974, about 10 to 15 years after the atmospheric nuclear weapons tests of the late 1950s and early 1960s. The new ^{14}C produced by the bomb tests significantly elevated prebomb $\Delta^{14}C$ levels in the atmosphere and upper ocean and made postbomb $\Delta^{14}C$ observations more difficult to interpret. *Quay et al.* [1983], using a 1979 transect of ^{14}C data that clearly resolved the upper thermocline layers north and south of the equator, found that the upper thermocline water masses feeding the equatorial upwelling actually had higher levels of $\Delta^{14}C$ (i.e., more bomb contamination) than the local surface water. *Quay et al.* argued that a deep source of uncontaminated or weakly contaminated water was needed to dilute $\Delta^{14}C$ levels in the water being upwelled from shallow depths. Using a mass balance derived from a two-dimensional model, they suggested that the equatorial upwelling had to draw up a small amount of water as cool as 11° or 12°C from 250–300 m in the lower thermocline in order to satisfy the $\Delta^{14}C$ constraint.

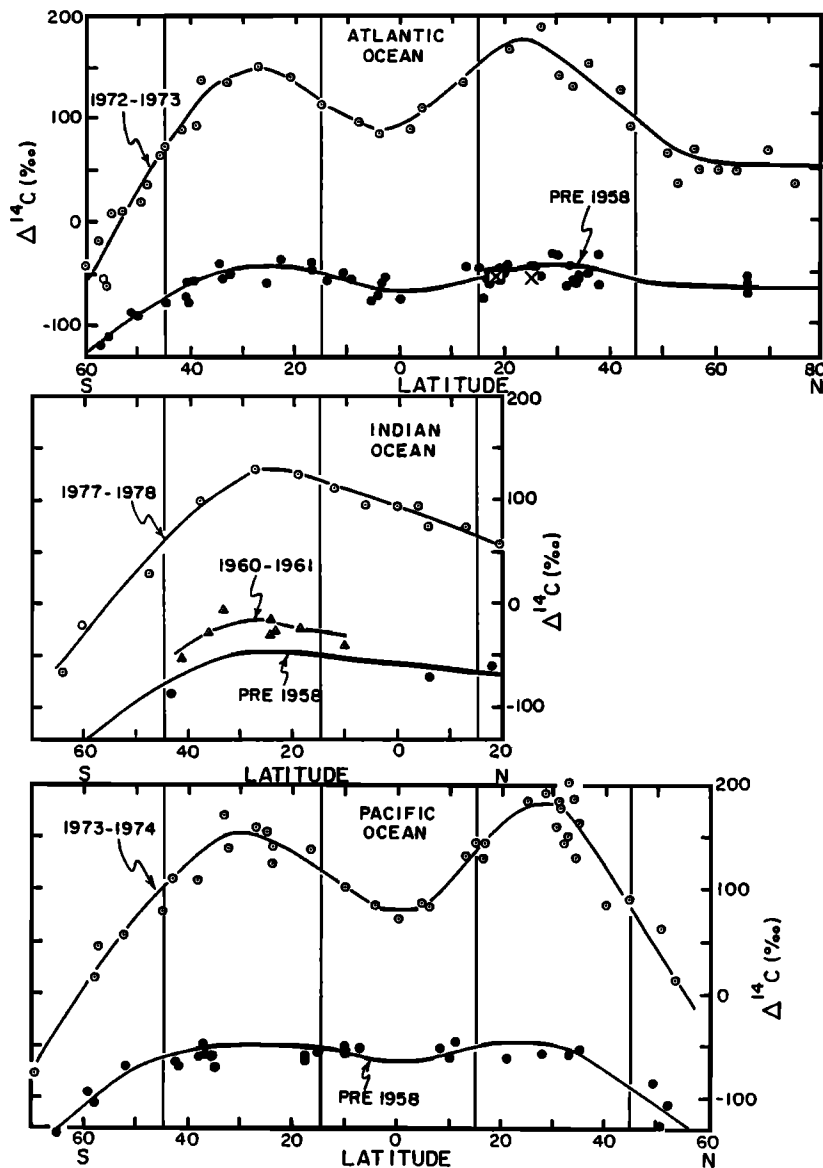The easterly wind stress at the equator is strongest in the central Pacific [*Wyrtki*, 1975], such that by far the largest

Fig. 1. Summary of surface water $\Delta^{14}C$ measurements as a function of latitude during the prebomb era and at the time of the GEOSECS surveys. Copied from *Broecker and Peng* [1982].

amount of upwelling occurs in the center of the basin [*Philander et al.*, 1987]. However, the equatorial thermocline slopes upward toward the east, allowing the layers of the lower thermocline to come closest to the surface in the far eastern Pacific. In fact, it is quite possible to reinterpret *Quay et al.*'s [1983] $\Delta^{14}C$ constraint in terms of lower thermocline water upwelling off the coast of South America. Rather than call for the direct upwelling of 11° or 12°C water to the surface via the equatorial divergence, Quay et al. could have proposed that surface currents advect upwelled low-$\Delta^{14}C$ water from the east into the center of the basin. The coastal region off the coast of Peru between 4° and 15°S is a well known source of unusually cold upwelled water. During cold events of the El Niño–Southern Oscillation (ENSO), water as cold as 14°C is detected at the surface at 7°S [*Wyrtki*, 1975]. *Broecker and Peng* [1982] and *Druffel* [1987] have discussed the possibility that the upwelling off Peru is the source of the low-$\Delta^{14}C$ signal in the equatorial Pacific.

High nutrient levels in surface water, like low $^{14}C/^{12}C$ ratios, indicate the presence of recently upwelled water. Figure 2 shows a map of the time-averaged surface nitrate distribution in the tropical Pacific. Surface waters with high concentrations of nitrate form a tongue which extends westward from the coast of Peru. The high nitrate tongue is not centered around the equator. It remains distinctly south of the equator out to 150°W. The position of the high-nitrate tongue gives the impression that upwelled water off Peru spreads to the west as a distinct water mass that is chemically distinguishable from the water masses upwelling along the equator. Indeed, current vectors from equatorial circulation models show that surface water south of the equator in the eastern Pacific moves primarily in a westward direction [*Philander et al.*, 1987]. This is due to the fact that the wind stress in the region has a large northward component which allows surface currents veering off to the left of the wind to move nearly due west. The wind stress also intensifies away
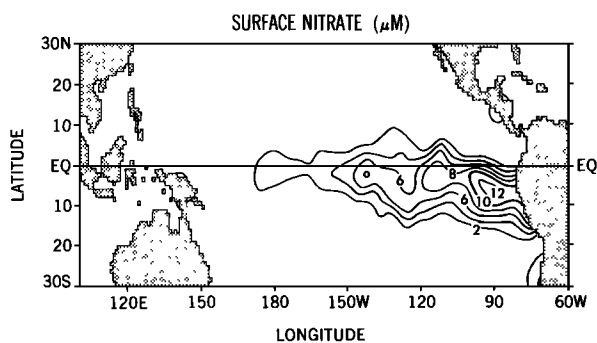
SURFACE NITRATE (μM)

Fig. 2. Surface distribution of nitrate in the equatorial Pacific as mapped from data collected at all times of the year. Data set provided by S. Levitus, R. Najjar, and J. L. Reid (personal communication, 1990).

from the coast, thereby creating additional upwelling in the open sea west of Peru.

Unusually high partial pressures of CO_2 are observed south of the equator in the eastern Pacific in keeping with what one expects from the warming of upwelled water which is initially quite cold. *Keeling* [1968] reports oceanic pCO_2 levels off the coast of Peru that greatly exceed pCO_2 levels measured along the equator. A transect of pCO_2 measurements reported by *Murphy et al.* [this issue] shows that the pCO_2 maximum south of the equator extends to at least 110°W. Most of the discussion in the geochemical and biological literature about upwelling in the equatorial Pacific is focused on the equatorial divergence [e.g., *Quay et al.*, 1983; *Chavez and Barber*, 1987]. But as the nitrate and CO_2 distributions illustrate, this is not the whole story. Because of its deeper origin, the water upwelling in the east has much higher nitrate and ΣCO_2 concentrations than the water upwelling along the equator. It appears to be an important and unappreciated component of chemical budgets in the tropical Pacific.

The object of this paper is to characterize the larger oceanographic context in which the upwelling off Peru occurs. Hydrographic relationships to be reviewed below clearly show that the upwelled water mass originates in the lower layers of the Equatorial Undercurrent. It appears to travel all the way across the Pacific basin from the western South Pacific. The flow in the lower layers of the undercurrent and the upwelling off Peru also appear to be the final steps of a large-scale ventilation process which begins in the circumpolar region and extends through the entire South Pacific thermocline. This feature has not been documented before for two reasons. First, the temperature and density of the water upwelling off Peru are significantly warmer and lighter than the thermocline water masses forming in the circumpolar region. No such connection can be drawn using an isopycnal or density-conserving flow trajectory. Second, this feature is not reproduced by global-scale ocean circulation models. In fact, the high-latitude origin of the water upwelling off Peru is best appreciated by analysis of the prebomb distribution of $\Delta^{14}C$ as preserved in old seawater measurements from the late 1950s and in the dated growth bands of old coral heads.

Before we proceed to the body of this paper, a few comments about ^{14}C nomenclature and systematics are in order. Radiocarbon measurements are reported as $\Delta^{14}C$, which is defined as a deviation, in parts per thousand or per

mil (‰), of the $^{14}C/^{12}C$ ratio in a sample from the $^{14}C/^{12}C$ ratio in an isotopic standard. The international $^{14}C/^{12}C$ standard ratio, designated as 0‰, can be thought of as the $^{14}C/^{12}C$ ratio in the preindustrial atmosphere. Isotopic ratios reported using the $\Delta^{14}C$ notation are normalized for isotope fractionation due to air-sea CO_2 exchange and biological uptake by the measurement of the $^{13}C/^{12}C$ ratio in all samples. A water parcel isolated from the atmosphere loses ^{14}C at a rate of 10‰, or 1%, per 80 years due to radioactive decay. Measurement errors for $\Delta^{14}C$ measurements are typically 3 to 8‰. A coral growth band accreted from seawater before the bomb tests typically contains about 50‰, or 5%, less ^{14}C than a preindustrial sample of atmospheric CO_2 with the same amount of carbon. The small excess of ^{14}C in the atmosphere during preindustrial time allowed enough ^{14}C to pass across the air-sea interface to balance the decay of ^{14}C throughout the ocean.

Like $\Delta^{14}C$, many geochemical tracers (e.g. nitrate, phosphate, silica, and ΣCO_2) are good tracers of upwelling because of their steep vertical gradients below the surface mixed layer. However, the high subsurface concentrations and steep vertical gradients of most geochemical tracers are produced biologically. The vertical fluxes of organic matter giving rise to these characteristics are subject to poorly characterized surface processes. The subsurface distribution of $\Delta^{14}C$ is characterized by a ^{14}C deficit produced by radioactive decay. Biological processes have very little effect on $\Delta^{14}C$. Thus the $\Delta^{14}C$ distribution is much easier to interpret and is much easier to simulate in models.

Furthermore, surface $^{14}C/^{12}C$ levels are modified by interaction with the atmosphere very, very slowly. *Broecker and Peng* [1974] showed that the equilibration of carbon isotopes between the mixed layer of the ocean and the atmosphere takes about 10 years. This is much slower than the equilibration time scale for temperature or other gases ($\sim$1 month). Thus an upwelled water mass can be warmed up fairly quickly by taking up heat from the atmosphere, but it may travel tens of thousands of kilometers before its $^{14}C/^{12}C$ ratio changes very much. The weak coupling between $^{14}C/^{12}C$ ratios in the atmosphere and surface ocean turns out to be a very useful property.

Murray et al. [1989] report that the downward flux of nitrogen in sinking organic particles in the eastern equatorial Pacific is about 0.25 mol N m^{-2} yr^{-1}. This information allows one to compute a rough residence time for the nitrate in the high-nitrate tongue of Figure 2 of about 1 year (0.01 mol N m^{-3} × 30 m ÷ 0.25 mol N m^{-2} yr^{-1}). The 1-year residence time for nitrate accounts for the ability of nitrate upwelled off Peru to spread laterally for thousands of kilometers to the west. The distinction between the 1-year residence time for nitrate and the 10-year equilibration time for $\Delta^{14}C$ should alert the reader to the possibility that the upwelling signal in the surface $\Delta^{14}C$ distribution will be 10 times more persistent than the nitrate signal! Because the isotopic signature of the upwelled water off Peru is so distinct, the surface distribution of $\Delta^{14}C$ essentially maps the territory visited by Peruvian water during the 10 years following its appearance at the surface.

In addition to the perturbation caused by the bomb tests, $\Delta^{14}C$ levels have been altered by the burning of fossil fuels, which release $^{12}CO_2$, but no $^{14}CO_2$, to the atmosphere. Between the late 1800s and 1950, atmospheric $\Delta^{14}C$ levels were observed to decline by about 20–25‰. The decline in
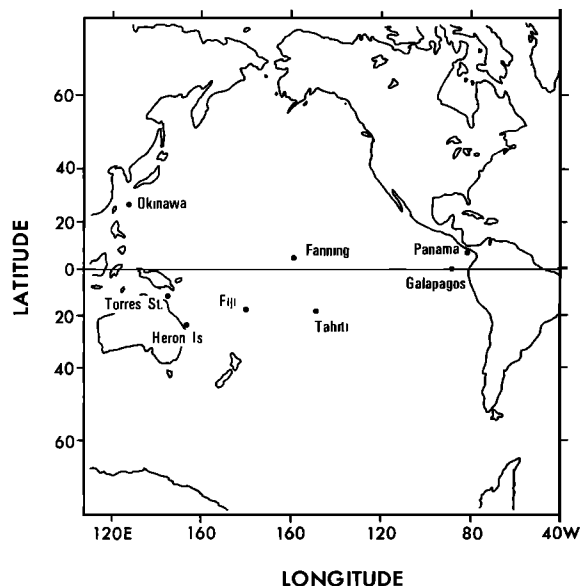
Fig. 3.   Map of the Pacific basin showing the locations of coral and shell sites used in this study.

atmospheric $\Delta^{14}C$ levels between 1900 and 1950 is known as the "Suess effect" [*Suess*, 1955; *Stuiver and Quay*, 1981]. The Suess effect is a small perturbation compared with the perturbation from the bomb tests but is an important factor in our study. The magnitude of the Suess effect in surface waters of the North Atlantic and North Pacific is typically about half that recorded in the atmosphere, i.e., about 10–13‰, due to the dilution of the fossil CO_2 input to the ocean by the large quantities of dissolved CO_2 in and above the main thermocline. E. Druffel (personal communication, 1990) has documented the fact that the oceanic Suess effect in the South Pacific is much smaller than that in the North Pacific or North Atlantic. This observation is puzzling but can be understood, perhaps, by the mechanism proposed here for the ventilation of the South Pacific thermocline.

In an appendix to this paper we tabulate a set of coral $\Delta^{14}C$ measurements which were produced at Lamont-Doherty Geological Observatory (LDGO) over the last 10 years (Table A3). Some of the data in Table A3 are used in this study. We have also compiled a post-1950 global coral $\Delta^{14}C$ data set for use in model validation exercises (Table A1). The data in Table A1 document the temporal evolution of surface ocean $\Delta^{14}C$ levels at 18 locations through all or part of the nuclear era.

CORAL OBSERVATIONS

Head-forming corals grow in the upper 10 m of the ocean. Their annual growth bands can be analyzed to reconstruct past chemical properties of the surface ocean [*Knutson et al.*, 1972]. There are six locations in the tropical Pacific where the $CaCO_3$ from annual coral growth bands has been analyzed for prebomb levels of $\Delta^{14}C$, Okinawa, Uva Island (west coast of Panama), Fanning Island, Galapagos, Fiji, and Heron Island (east coast of Australia). Figure 3 shows the location of the prebomb sites. Table 1 lists the average $\Delta^{14}C$ for the 1949–1955 annual growth bands of the six corals. Figure 4 shows $\Delta^{14}C$ levels for individual growth years at four of the sites, Okinawa, Fanning, Fiji, and Galapagos, between 1938 and 1958. Several of the corals date back to the turn of the century. Average values for "pre-1920" growth bands are also given in Table 1. Because the data reported in Table 1 represent multiyear averages of individual measurements, the error associated with the average is in no case worse than ±3‰.

In addition to the corals there are two sites, Torres Strait (NE Australia) and Tahiti, where mollusk shells were collected live at known times in the past and were measured for $\Delta^{14}C$. Table 1 lists the shell data and gives the year of collection. Figure 3 shows the locations of these sites. Mollusk shell data represent an average $\Delta^{14}C$ content over the years the shell grew. Errors on the shell measurements are about ±5‰.

The summary plot of surface $\Delta^{14}C$ seawater measure-

TABLE 1.   Reconstruction of the Pre-1920 Ocean-Atmosphere $\Delta^{14}C$ Gradient From Banded Corals and Dated Shells

Site	Prebomb Average 1949–1955	Ocean Suess Effect*	Pre-1920†	Pre-1920 Ocean-Atmosphere Difference‡	Model	Data-Model Difference	Reference
			Corals				
Okinawa	−42	−13	−29	−23	−33	+10	*Konishi et al.* [1982]
Panama	−58	(−10)	(−48)	−42	−50	+8	*Druffel* [1987]
Fanning	−59	(−10)	(−49)	−43	−52	+9	*Druffel* [1987]
Galapagos	−72	−6	−66	−60	−53	−7	*Druffel* [1981]
Fiji	−60	(−3)	(−57)	−51	−39	−12	*Toggweiler* [1983]
Heron Island	−50	+3	−53	−47	−38	−9	E. Druffel (personal communication, 1990)
			Shells				
Torres Strait§			−54	−48	−35	−13	*Gillespie and Pollach* [1979]
Tahiti‖	−62	−4	−58	−52	−45	−7	*Broecker and Olson* [1961]

*Figures given indicate the magnitude of the local Suess effect. Figures without parentheses represent the measured $\Delta^{14}C$ difference between 1900 and 1950. Figures with parentheses are estimates based on measured 1900–1950 $\Delta^{14}C$ differences in adjacent corals.

†Figures without parentheses represent single measurements or averages of coral or shell data from 1850–1920. Figures with parentheses are estimates based on prebomb coral averages (column 1) from which the Suess effect (column 2) has been subtracted.

‡Late nineteenth to early twentieth century atmospheric $\Delta^{14}C$ levels were about −6‰ [*Stuiver and Quay*, 1981]. In order to compare model results derived from an assumed atmospheric level of 0‰ with pre-1920 coral and shell data, we have added 6‰ to the coral and shell values in column 3 to arrive at a pre-1920 ocean-atmosphere $\Delta^{14}C$ difference.

§Average of three shells, two collected in 1875 (−58 and −56‰), one in 1909 (−49‰).

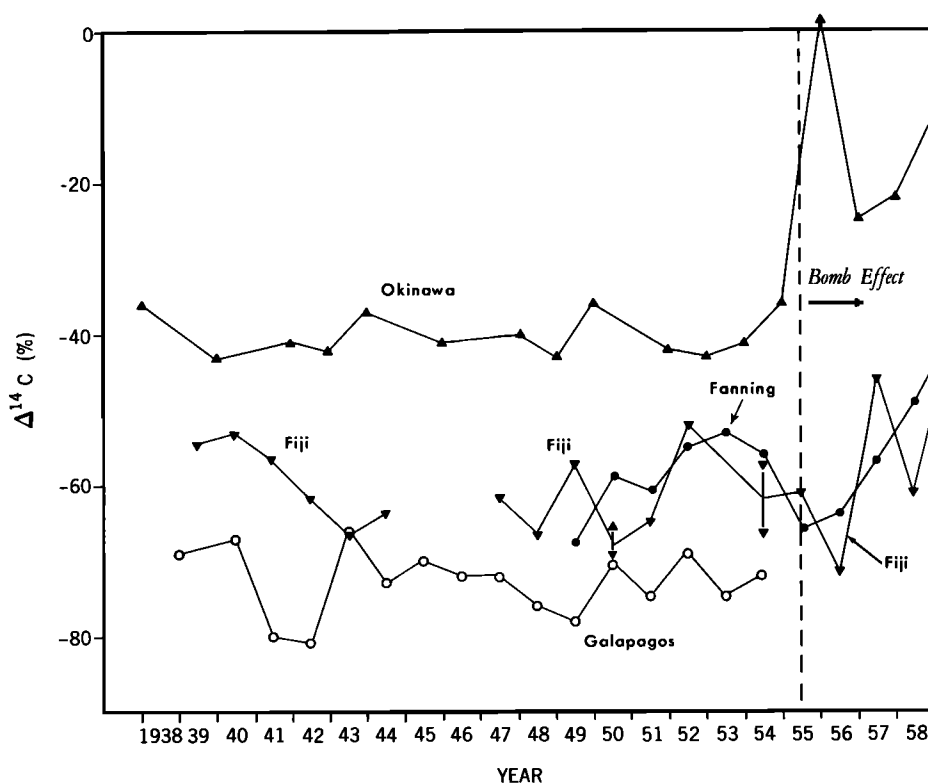‖Two dated shell samples from Tahiti appear in this reference, one collected in 1883 (−58‰), the other in 1957 (−62‰).

Fig. 4. Time evolution of $\Delta^{14}C$ in the Okinawa, Fiji, Fanning, and Galapagos corals between 1938 and 1958 showing interannual variability and the beginning of the bomb effect. Okinawa data are reported by *Konishi et al.* [1982]. Fiji data are reported by *Toggweiler* [1983] and in Table A3. Fanning data are reported by *Druffel* [1987]. Galapagos data are reported by *Druffel* [1981].

ments in Figure 1 includes a compilation of "pre-1958" seawater measurements made during the early years of the postbomb era. Many of these early seawater samples were already contaminated with bomb ^{14}C when collected. Figure 4 shows that oceanic $\Delta^{14}C$ levels at the four Pacific coral sites were essentially flat until a large jump is recorded at Okinawa in 1956 due to the bomb effect. A bomb-induced rise in southern hemisphere $\Delta^{14}C$ levels (Fiji) does not become apparent until 1957, and perhaps not until 1959. The first appearance of bomb ^{14}C in the South Pacific lags the first appearance in the north because all the large U.S. and Soviet bomb tests were conducted in the northern hemisphere.

The Galapagos Islands are located between the equator and 1°S, just north of the tongue of cold 19°–20°C water which extends westward from the coast of South America in maps of the sea surface temperature climatology for the late summer–early fall [*Robinson*, 1976; *Wyrtki*, 1981]. It is therefore not surprising that the lowest $\Delta^{14}C$ level among the eight sites in Table 1 is found in the Galapagos coral [*Druffel*, 1981]. Galapagos $\Delta^{14}C$ levels between 1949 and 1955 averaged −72‰. The −72‰ prebomb average represents an extraordinarily low ΔC value for surface water. Prebomb $\Delta^{14}C$ levels this low are typical of thermocline water at 500–700 m in the subtropics.

The second and third lowest prebomb $\Delta^{14}C$ levels in Table 1 come from southern hemisphere sites at the fringes of the tropical zone, i.e., a shell collected in Tahiti (−62‰) and the Fiji coral (−60‰). The fact that $\Delta^{14}C$ levels at these sites are similar to or perhaps lower than $\Delta^{14}C$ levels at Fanning Island (−59‰) is remarkable. $\Delta^{14}C$ levels at Fanning Island

are characteristic of water upwelling via the equatorial divergence [*Druffel*, 1987]. Given that water flowing slowly toward Tahiti and Fiji is continually picking up ^{14}C from the atmosphere, the low $\Delta^{14}C$ levels observed at Tahiti and Fiji cannot come from the divergence. These levels can come only from a source with a lower initial $\Delta^{14}C$ content, like the Peru upwelling. The highest $\Delta^{14}C$ level among the eight sites is recorded in the northern hemisphere at Okinawa (−42‰).

One of the most critical questions for this analysis concerns the degree to which *Druffel*'s [1981] Galapagos coral recorded the actual prebomb $\Delta^{14}C$ content of water upwelling off Peru. Even though the Galapagos region is bathed in nutrient-rich Peruvian water most of the time, it is subject to seasonal excursions of low-salinity, low-nutrient water from the north [*Wyrtki et al.*, 1976]. These excursions are responsible for the displacement of the high-nitrate tongue in Figure 2 to a position south of the islands in this annual composite. They would also tend to introduce relatively high $\Delta^{14}C$ levels found in northern hemisphere water into annual coral growth bands and thereby influence the $\Delta^{14}C$ record. The lowest $\Delta^{14}C$ level recorded in any of the Galapagos growth bands is −81‰ (1942). It is quite possible that the lowest $\Delta^{14}C$ level recorded by the Galapagos coral is the $\Delta^{14}C$ level most representative of the Peru upwelling.

These excursions of northern hemisphere water into the Galapagos region are most pronounced during El Niño events when the cold upwelling off Peru also ceases. If it were possible to identify El Niño years in the prebomb Galapagos record, one might simply remove these years from the prebomb average. One could then assume that the correspondence between the remaining Galapagos growth
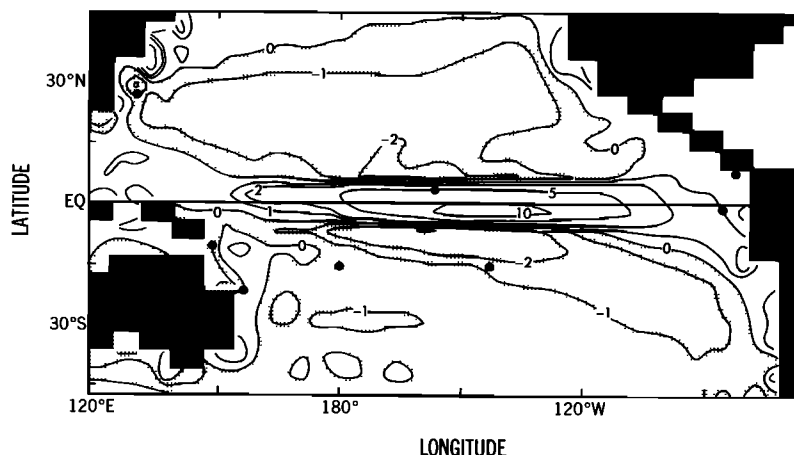
Fig. 5.   Vertical velocities at 51 m in the tropical Pacific according to the *Toggweiler et al.* [1989a] model. Contours have been drawn at $-5, -2, -1, 0, 1, 2, 5$, and 10×10^{-4} cm s^{-1}. Vertical motions are downward in the stippled regions. Locations of coral and shell sites on the model grid are indicated by the solid dots.

bands and the Peru upwelling would be much improved. Unfortunately, the prebomb Galapagos record in Figure 4 does not show any obvious correlation with ENSO.

Druffel's [1981] prebomb Galapagos record comes from a coral head which grew in Urvina Bay off the west coast of Isabela Island. The record ends in 1954 when Urvina Bay was suddenly lifted above sea level by a volcanic disturbance [*Colgan and Malmquist*, 1987]. *Druffel* [1981, 1987] report postbomb Δ^{14}C data from two additional Galapagos corals collected at different locations (Hood Island and Santa Cruz Island), which show large 20 to 30‰ positive Δ^{14}C excursions during five separate El Niño events between 1965 and 1982. The Hood Island and Santa Cruz Island records do not extend back beyond 1961. Thus, either El Niño-induced Δ^{14}C variations were too small during prebomb time to influence the Δ^{14}C content of an annual growth band, or the location of Urvina Bay was a factor in muting El Niño variations at the prebomb site.

The west coast of Isabela Island and Urvina Bay face the open sea to the west. Isabela Island is the largest of the Galapagos Islands and is known to deflect the waters of the Equatorial Undercurrent upward [*Robinson*, 1987]. Surface temperatures as low as 16°–18°C are observed to the west of the island. The water upwelling off Peru also has its origin in the Equatorial Undercurrent [*Wyrtki*, 1963], such that an Urvina Bay coral might provide a more direct record of the Peru upwelling than is obvious at first glance. This argument would be more convincing if prebomb Δ^{14}C levels at Urvina Bay were systematically lower than at the other sites. This cannot be determined from the available data.

Given all the uncertainties, the most reasonable inference we can make is that the actual prebomb Δ^{14}C content of the water upwelling off Peru was probably somewhere between the $-72‰$ prebomb average for the Urvina Bay coral and the $-81‰$ minimum value.

Comparison of Coral Records With a General Circulation Model ^{14}C Simulation

Because the number of prebomb Δ^{14}C data points is so small, it is extremely helpful to compare these values with a Δ^{14}C surface distribution predicted by a three-dimensional ocean circulation model [*Toggweiler et al.*, 1989a, b]. The

ocean model described by Toggweiler et al. is a standard primitive equation model of the type developed at the Geophysical Fluid Dynamics Laboratory (GFDL) [*Bryan and Lewis*, 1979]. It is a global model with a coarse grid (4.5° of latitude × 3.75° of longitude × 12 vertical levels) which is forced by annual mean winds, and annual mean surface temperatures and salinities.

The model radiocarbon simulations of *Toggweiler et al.* [1989a, b] were designed as model validation exercises in which model Δ^{14}C distributions could be compared with the global GEOSECS data set. The initial simulation was run out with a fixed atmospheric boundary condition until its Δ^{14}C distribution reached steady state. The model's deepwater distributions were then compared with subthermocline Δ^{14}C observations that had not been affected by bomb ^{14}C [*Toggweiler et al.*, 1989a]. Next, the atmospheric boundary condition for Δ^{14}C was perturbed to simulate the bomb effect. Model output was compared with the upper ocean Δ^{14}C distributions at the time of GEOSECS [*Toggweiler et al.*, 1989b]. The present paper explores a realm of model output that the original papers did not deal with in much detail, namely, the surface Δ^{14}C distribution under steady state conditions.

Figure 5 shows a map of the model's vertical velocities at 51 m, the base of layer 1. Locations of the eight coral and shell sites in Table 1 are indicated with large solid dots. The model's maximum upwelling straddles the equator in the central Pacific where the easterly wind stress is greatest. The maximum upwelling rate is about 300 m yr^{-1}. Upwelling rates off the coast of South America are about one-tenth the maximum rates in the center of the basin. According to the model, coral and shell locations along the perimeter of the western Pacific (Okinawa, Torres Strait, and Heron Island) are bathed in water influenced by model boundary currents which have their origin in the tropical zone. Surface flows originating in the upwelling zone reach the locations of Tahiti and Fiji after a few years of slow southwesterly drift.

In order to directly compare the model and the coral data a few accommodations are necessary to make the coral data reflect the same steady state conditions which are driving the model. The prebomb Δ^{14}C simulation of *Toggweiler et al.* [1989a] is forced by a uniform atmospheric ^{14}C/^{12}C ratio of
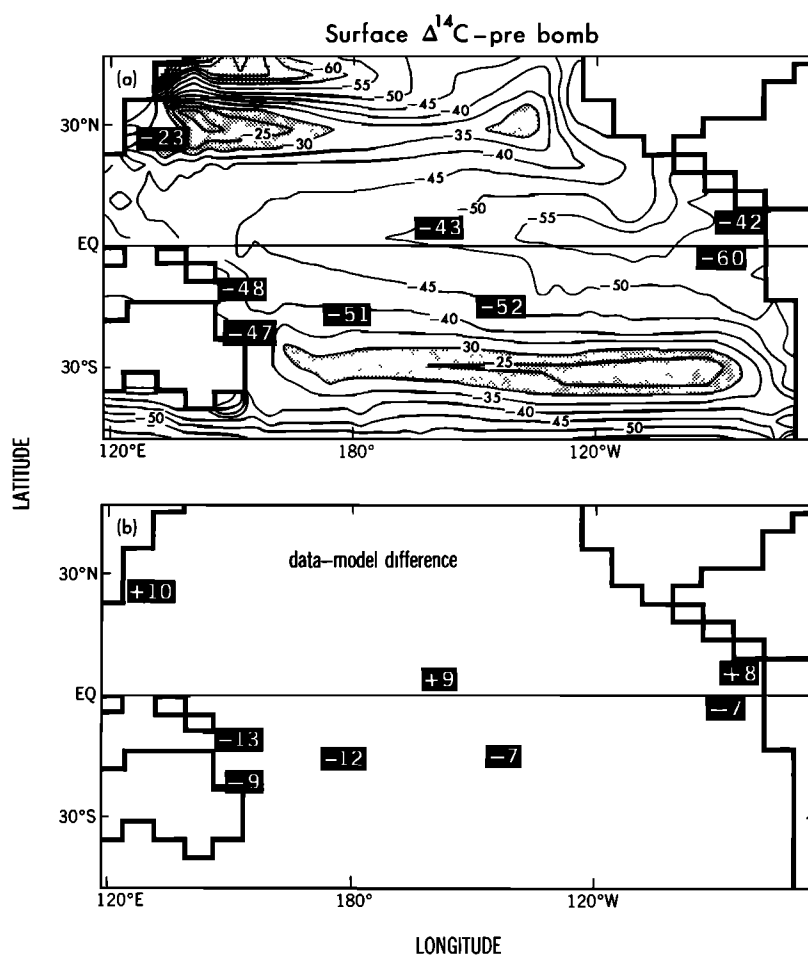
Fig. 6. (a) Prebomb surface $\Delta^{14}C$ distribution (per mil) predicted by the Toggweiler et al. [1989a] model overlaid with $\Delta^{14}C$ observations from corals and shells listed in Table 1 (white-on-black characters). Model contours represent an equilibrium solution for a steady, 0‰ atmospheric $\Delta^{14}C$ boundary condition. In order to be consistent with model output, coral and shell data have been modified to reflect the ocean-atmosphere $\Delta^{14}C$ gradient between 1850 and 1920 (Table 1). (b) Difference between coral data and the model at the coral sites.

0‰, which is held steady for the duration of a 2000-year run. Unfortunately, atmospheric $\Delta^{14}C$ levels have not been completely steady for the last 2000 years. The part of the record one would most like to avoid is the first half of the twentieth century, when $\Delta^{14}C$ levels were declining as a result of the Suess effect. Atmospheric $\Delta^{14}C$ levels were relatively stable between 1850 and 1920 at about −6‰ [Stuiver and Quay, 1981; Druffel and Suess, 1983]. We assume that the time period between 1850 and 1920 represents the closest natural counterpart to the steady forcing used in running the model.

In columns 2–4 of Table 1 some "corrections" are applied to the data in column 1 in order to reproduce the ocean-atmosphere $\Delta^{14}C$ gradient between 1850 and 1920. Where long coral records or old shell data exist, column 3 simply lists averages of pre-1920 data (Okinawa, Galapagos, and Heron Island corals, and Torres Strait and Tahiti shells). Pre-1920 data are not available for three of the corals. We therefore attempt to adjust the 1949–1955 prebomb levels in column 1 for the Suess effect using information about the local Suess effect in the longer records.

The magnitude of the Suess effect in the Pacific Ocean has a north-south trend, with the greatest change recorded in Okinawa (a −13‰ change from 1900 to 1950) and much smaller changes in the southern hemisphere (−6‰ in the

Galapagos coral, +3‰ in the Heron Island coral, and a −4‰ difference between Tahitian shells collected in 1883 and 1957). In light of this trend, we assume that a −10‰ fossil fuel dilution effect applies at the northern hemisphere sites with short records (Panama and Fanning), and assume that a −3‰ dilution effect applies at Fiji. Column 3 includes a Suess effect–corrected value for each of the three short coral records. The changes in northern hemisphere $\Delta^{14}C$ levels caused by the variable Suess effect produce an even larger spread between northern and southern hemisphere $\Delta^{14}C$ levels than is evident in 1949–1955.

The fourth column of Table 1 shows a "pre-1920 ocean-atmosphere $\Delta^{14}C$ difference" which can be directly compared with model output. Column 5 shows model results at the eight sites. Column 6 shows the data-model difference at the eight sites. Figure 6a shows the prebomb surface $\Delta^{14}C$ distribution predicted by the model. Overlaid on the model contours are the pre-1920 ocean-atmosphere $\Delta^{14}C$ differences from Table 1 in discrete white-on-black numbers.

The model's circulation field seems to do a reasonably good job accounting for the $\Delta^{14}C$ differences between the corals due to their location and distance from the upwelling zone. However, there is a systematic offset between corals in the northern and southern hemispheres which the model
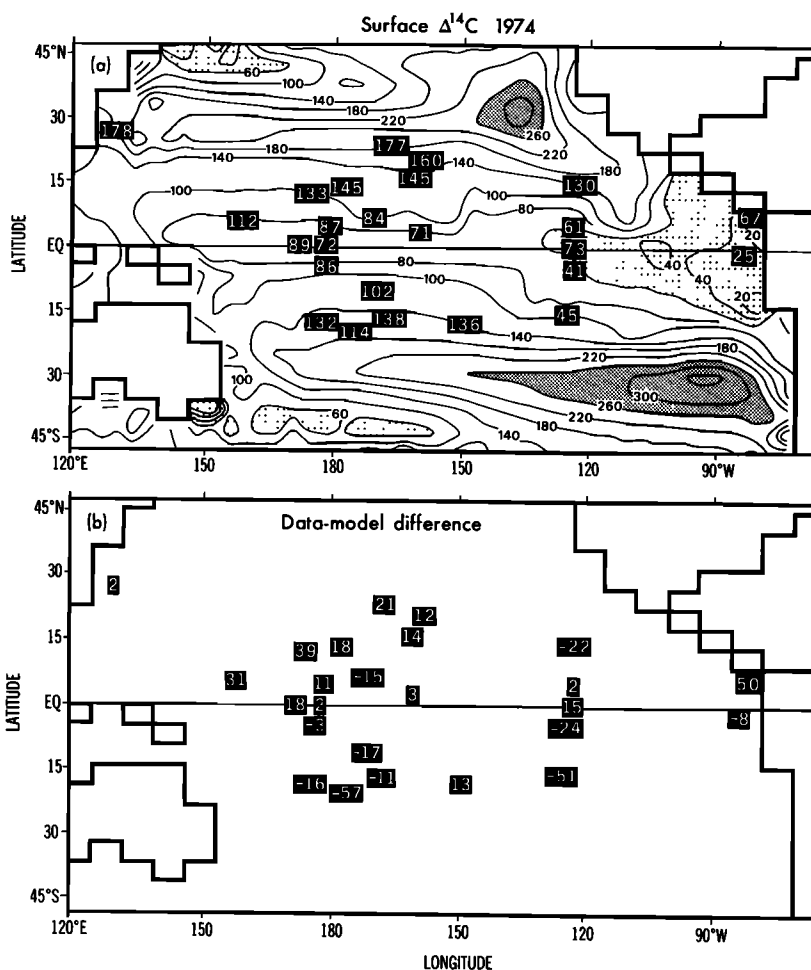
Fig. 7. (a) Surface $\Delta^{14}C$ distribution (per mil) in 1974 predicted by the *Toggweiler et al.* [1989b] model overlaid with GEOSECS seawater observations [*Ostlund et al.*, 1987] and coral measurements from 1974 growth bands. Observations are given by white-on-black characters. Coral data are listed in Table A1 along with sources. The model $\Delta^{14}C$ simulation was forced by a time history of atmospheric $\Delta^{14}C$ measurements for the period 1950-1990 which was partitioned into three latitude bands in order to capture the disparity between the northern and southern hemispheres in the years immediately following the bomb tests [see *Toggweiler et al.* [1989b, Figure 1]. (b) Difference between GEOSECS and coral data and the model.

does not reproduce. Figure 6b plots the differences between the coral and shell data and the model listed in column 6 of Table 1. Observed northern hemisphere $\Delta^{14}C$ levels are in every case higher than the model by 8 to 10‰, while the observed southern hemisphere values are lower by about the same amount.

Errors introduced in making the corrections in Table 1 are hard to estimate. It is entirely possible that the combined errors due to the $\Delta^{14}C$ measurements themselves and the corrections in Table 1 could be as large as ±8‰. Thus the data-model difference at any particular location in Figure 6b may be only marginally significant. On the other hand, the average data-model difference within each hemisphere and the 15-20‰ $\Delta^{14}C$ differences between the hemispheres do convey real information.

The coral data suggest that the spreading of water with the lowest $\Delta^{14}C$ content is largely confined to the southern hemisphere. This would seem to be due to the fact that the "oldest" upwelled water upwells to the surface off South America and then remains south of the equator as in the nitrate distribution in Figure 2. It will be shown below that the upwelling of low-$\Delta^{14}C$ water in the model is associated

with the upwelling along the equator, which tends to distribute the low-$\Delta^{14}C$ signature evenly between the hemispheres. The model seems to upwell roughly the right amount of low-$\Delta^{14}C$ water, but not at the right place.

After the large U.S. and Soviet bomb tests in 1961 and 1962, atmospheric $\Delta^{14}C$ levels rose dramatically. During the decade between the end of the bomb tests and the beginning of GEOSECS, the ocean-atmosphere $\Delta^{14}C$ gradient averaged about 500‰, when it had been only 40-50‰ before. Figure 7a shows a map of surface $\Delta^{14}C$ levels generated by the model for 1974, the year marking the midpoint of the Pacific GEOSECS expedition, 11 years after the end of the bomb tests. GEOSECS surface observations and coral observations at 12 sites (Table A1), are overlaid on the model results as discrete white-on-black numbers, as in Figure 6.

Figure 7b shows data-model differences at the locations of the observations. Again, one sees a systematic bias in the data-model difference between the hemispheres. North of the equator observed $\Delta^{14}C$ levels are about 15-20‰ higher on average than the model, while south of the equator, observed $\Delta^{14}C$ levels are roughly 30‰ lower. Again, the model appears to upwell relatively uncontaminated water

along the equator which dilutes bomb ^{14}C input in both hemispheres. The data-model differences suggest that the dilution should be much stronger south of the equator.

Figure 7 includes a great deal more data points than were available for the prebomb comparison in Figure 6. In particular, there is more information in the eastern Pacific, closer to the low-Δ^{14}C upwelling zone. The Galapagos coral again displays the lowest Δ^{14}C observation for this time frame. Model Δ^{14}C levels from the vicinity of the Galapagos Islands are within 8‰ of the Galapagos coral. However, the model predicts that Δ^{14}C levels north of the equator should be similar to Δ^{14}C levels south of the equator, when, in fact, a very sharp difference is observed between the Galapagos and Panama corals [Druffel, 1987]. The lowest Δ^{14}C levels observed along the eastern Pacific GEOSECS track (125°W) are not right at the equator, as in the model, but are 5° to 15° south of the equator, where the observed values are only +41 and +45‰. This pattern is consistent with the nitrate and CO$_2$ information discussed in regard to Figure 2.

Coral Time Series

While most of the analysis of coral Δ^{14}C records thus far has been based on averages of annual growth bands, there is another signal to be found in the interannual variations among the yearly bands. During the 1950s the time histories of the Okinawa, Fiji, and Fanning corals are complete enough to illustrate that an anticorrelation exists between Δ^{14}C levels at Fiji and Fanning, and Δ^{14}C levels at Okinawa (Figure 4). Δ^{14}C levels are low at Okinawa during 1952 and 1953 while they are high at Fiji and Fanning. The 1956 coral band from Okinawa has a Δ^{14}C content in excess of 0‰, while the 1956 band from Fiji shows a distinct minimum of -72‰.

The pattern of variability and the anti-correlation noted in Figure 4 appear to be coherent with the ENSO cycle. Figure 8 shows the Fiji and Okinawa data replotted along with a record of the easterly wind stress in the central equatorial Pacific from Wyrtki [1975]. Δ^{14}C lows at Fiji and Δ^{14}C highs at Okinawa coincide with stronger easterly winds along the equator. The 1956 event noted above coincides with the strongest equatorial winds and largest Southern Oscillation pressure index during the 1940s, 1950s, and 1960s [Quinn, 1974]. The strong easterly winds in 1956 would be expected to generate the greatest volume of upwelled water and the coldest sea surface temperatures in the eastern Pacific. Thus the low Δ^{14}C points in the Fiji record (and possibly at Fanning) appear to be tracking a primary upwelling signal, while the low Δ^{14}C points from Okinawa appear to track an upwelling signal which is 180° out of phase with the upwelling at the equator.

El Niño events in 1953 and 1957 [Quinn, 1974] appear to correlate with low Δ^{14}C levels at Okinawa and high Δ^{14}C levels at Fiji. The 1957 El Niño appears to produce a strong reversal in the rise in the bomb ^{14}C signal at Okinawa. Philander and Hurlin [1988] have pointed out that easterly trade winds were unusually strong near 12°N during the 1982-1983 El Niño, causing a large quantity of equatorial water to advect northward into the subtropical belt. At the same time the easterlies along the equator were weak and even changed direction for a few months. Philander and Hurlin suggest that the northward transport of equatorial water during El Niño events is a normal consequence of the
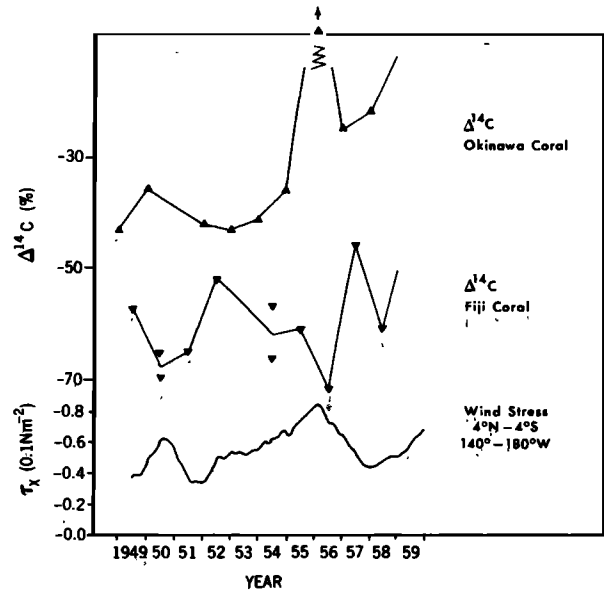
Fig. 8. Comparison of the time evolution of Δ^{14}C in the Okinawa and Fiji corals (Figure 4) between 1949 and 1959 with the observed zonal component of the wind stress in the central equatorial Pacific (4°N to 4°S, 140-180°W [after Wyrtki, 1975].

north-south migration of the Intertropical Convergence Zone (ITCZ) during the ENSO cycle. If true, it provides a simple explanation of the correlation between low Δ^{14}C levels at Okinawa and weak winds along the equator.

Errors for the Δ^{14}C measurements on individual growth bands are not small with respect to the amplitudes of these apparent ENSO wiggles. We hesitate to make too much out of the ENSO correlation in Figure 8. However, the time series records appear to add a new dimension to the time-averaged observations highlighted in Table 1 and in Figures 6 and 7. When conditions favor intense upwelling along the equator and the greatest upward slope in the thermocline toward the east, corals in the southern hemisphere and near the equator seem to record the upwelling of the coldest, deepest water. When conditions favor weak upwelling along the equator and stronger trade winds in the northern hemisphere, corals in the subtropical North Pacific appear to record an upwelling signal.

SUBSURFACE ORIGIN OF THE LOW-Δ^{14}C WATER

Maps of sea surface temperature and surface currents in the Pacific Ocean give one a superficial impression that the cool, high-nutrient water associated with the upwelling off Peru flows up from the south as part of the Peru Current. However, Wyrtki [1963] suggested that actual source of the upwelled water is the Equatorial Undercurrent (EUC), which flows toward South America from the west. Off the coast of South America there is a strong hydrographic front which divides warm, low-salinity, low-nutrient water from the northern hemisphere from the cool, high-salinity, high-nutrient water off Peru [Wyrtki, 1966]. On average, the front extends from the southern coast of Ecuador (~2°-4°S) to just north of the Galapagos Islands (~1°N). The upwelling of water with low ^{14}C/^{12}C ratios and high nutrient and CO$_2$ contents is clearly associated with the high-salinity water south of the front. Coastal water near the southern boundary

of Peru (18°S) is low in salinity like the water north of the equator and is not the source of the cool, high-nutrient water between 5° and 15°S.

Wooster and Gilmartin [1961] documented the existence of a southward flowing subsurface current along the coast of Peru, which they called the Peru-Chile Undercurrent (PCUC). *Wyrtki* [1963] and *Brockmann et al.* [1980] show that the flow of the PCUC is reduced considerably between 5° and 15°S owing to removal of water from the current by coastal upwelling. The reduction of the flow between 5° and 15°S is about 4×10^6 m^3 s^{-1} [*Wyrtki*, 1963]. The core of the southward flow is found at about 90 m and has a temperature of about 15°-16°C [*Brockmann et al.*, 1980]. *Wyrtki* [1963] speculated that part of the main Equatorial Undercurrent to the west of the Galapagos Islands splits off to the southeast to supply the upwelling off Peru and a major portion of the westward flow of the South Equatorial Current. *Lukas* [1986] confirmed this connection by tracing seasonal pulses in undercurrent water mass characteristics west of the Galapagos Islands to the coast of South America. Wyrtki also speculated that part of the undercurrent splits off to the north of the Galapagos Islands to supply the subsurface salinity maximum layer in the eastern tropical North Pacific. The high-salinity layer north of the equator remains submerged beneath an extensive low-salinity surface layer [*Reid*, 1969] and never reaches the surface.

Water forming the core of the Equatorial Undercurrent in the central Pacific does not reach South America. The core of the undercurrent is characterized by temperature-salinity (*T*-*S*) properties of roughly 20°-21°C and 35.2-35.4‰ [*Tsuchiya*, 1968]. According to *Bryden and Brady*, [1985] the warm, salty water in the core of the undercurrent becomes entrained into the surface flow between 110° and 95°W, i.e., to the west of the Galapagos Islands, and is drawn off to the north and south by the divergence along the equator. *Bryden and Brady* [1985] argue that the entrainment of 20°-21° water from the undercurrent into the surface layer is the origin of the "cold" tongue along the equator. Cooler and slightly fresher water from below the core of the undercurrent is the source for the high-salinity upwelled water off South America. Tsuchiya's maps indicate that water at the depth and temperature of the PCUC has salinities in the range 34.8-35.0‰.

Undercurrent water with the *T*-*S* properties of 11°-14°C and 34.8-35.0‰ forms a well-documented oceanographic feature known as the "Equatorial 13°C Water" [*Montgomery and Stroup*, 1962], which has become a focal point for studies of the undercurrent. The 11°-14°C water forms a thermostad in the equatorial thermocline which thickens to the east. *Tsuchiya* [1981] showed that the thickening is due to advection of water into the region from the west. He constructed maps of water properties along the 160 cL ton^{-1} steric anomaly surface (~26.45‰ in σ_θ) in order to trace the origin and fate of the 13°C Water. The 160 cL ton^{-1} isopycnal surface bisects the thermostad at a depth of 200 m at 105°W but does not outcrop at the surface off the coast of South America. Temperatures and densities characteristic of the very top of the thermostad are found at depths near 100 m off the coast of Peru [*Lukas*, 1986; *Tsuchiya*, 1968]. Analysis of the limited amount of prebomb Δ^{14}C (below) suggests that the 13° Water is, in fact, the source of the water upwelling off Peru.

Regional maps of water properties on the 200 cL ton^{-1} (~15°C) and the 160 cL ton^{-1} (~12.5°C) show high-salinity
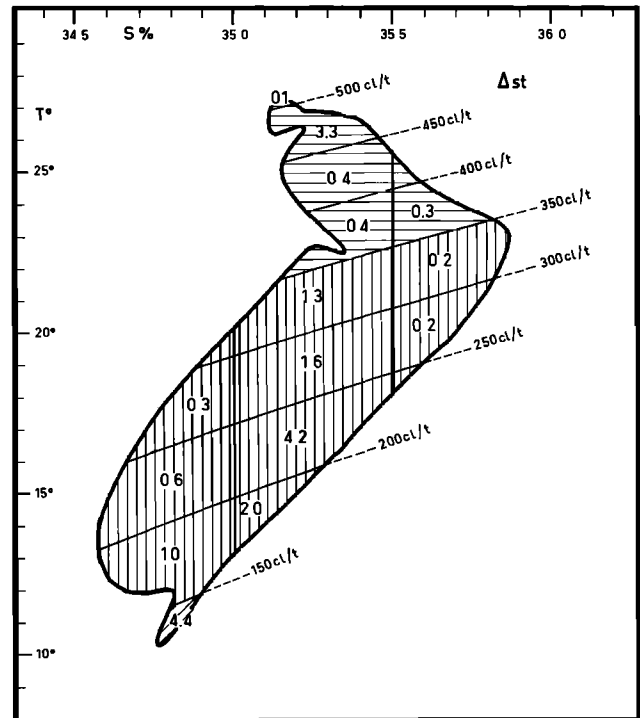
Fig. 9.　Eastward fluxes in the Equatorial Undercurrent at 170°E for various classes of thermosteric anomaly (units of 10^6 m^3 s^{-1}). Copied from *Rotschi* [1970].

and high-oxygen tongues extending northward to the equator in the western Pacific and eastward across the basin to the coast of South America [*Tsuchiya*, 1968]. Thus the lower part of the Equatorial Undercurrent appears to be formed from water masses in the South Pacific. This suggestion was confirmed by *Lindstrom et al.* [1987] who discovered the New Guinea Coastal Undercurrent flowing northward along the coast of Papua New Guinea up to the equator. The eastward flow of the Equatorial Undercurrent at 155°E (spanning a temperature range of 11°-22°C) is almost entirely accounted for by the northward flow of the New Guinea Coastal Undercurrent [*Tsuchiya et al.*, 1990].

The lower part of the Equatorial Undercurrent is a distinct mode of the undercurrent's transport [*Magnier et al.*, 1973; *Taft and Jones*, 1973; *Tsuchiya et al.*, 1990]. Figure 9, reproduced from *Rotschi* [1970] shows a *T*-*S* map for undercurrent water at 170°E, which apportions the flow into *T*-*S* components according to current meter measurements. The tiny appendage at the bottom of the *T*-*S* map represents an eastward flow of 4.4×10^6 m^3 s^{-1} associated with 11°C, 34.8‰ water. This is the largest component of the flow when the total undercurrent is apportioned among uniform density classes.

Δ^{14}C OBSERVATIONS IN THE EQUATORIAL UNDERCURRENT

While a conventional isopycnal analysis does not explicitly support the idea that the 13°C Water upwells off Peru, radiocarbon evidence suggests a direct connection. GEO-SECS Δ^{14}C observations from the lower thermocline in the tropical Pacific are reproduced in Table 2, which blends data from the report giving standard hydrographic and nutrient information [*Broecker et al.*, 1982] and the report giving the results of shore-based chemical analyses, including Δ^{14}C

TABLE 2. Tropical Pacific Hydrographic Data From GEOSECS Covering the Density Range of the Lower Undercurrent

Depth, m	θ, °C	Salinity, ‰	σ_θ, ‰	Oxygen	Silica	Phosphate	Nitrate	$\Delta^{14}C$, ‰	Comments
				Concentration, μmol kg^{-1}					
GEOSECS 257: 10.2°S, 170.0°W									
301	16.27	35.35	25.99	133	5.4	1.09	12.3		
322	15.13	35.14	26.08					−4.9	
377	12.03	34.88	26.53	105	14.7	1.65	21.9		0.10 TU
397	*11.03*	*34.78*	26.64					−72.5	
451	9.07	34.65	26.88	117	23.8	1.94	28.0		no ³H
497	8.09	34.60	26.99					−104.0	
601	6.31	34.53	27.18	123	39.4	2.23	33.5		
GEOSECS 251: 4.5°S, 179.0°E									
236	17.13	35.38	25.80					+34.5	
243	16.45	35.32	25.92	117	6.9	1.27	15.0		
274	13.10	35.03	26.43	95	14.2	1.66	22.1		0.15 TU
296	*10.88*	*34.83*	26.70					−72.3	
309	10.60	34.81	26.74	96	21.2	1.89	27.3		no ³H
361	9.52	34.72	26.85	96	25.7	2.01	29.8		
427	8.51	34.65	26.97	90	31.2	2.18	32.6		
497	8.05	34.54	26.95					−108.0	
506	7.77	34.61	27.04	97	34.8	2.26	33.6		
GEOSECS 246: 0.0°S, 179.0°E									
205	18.31	35.32	25.46	140	6.9	0.95	12.0		
210	···	35.31	···					+11.6	pump*
221	17.13	35.28	25.73	139	8.0	1.04	13.4		
242	15.10	35.11	26.07	141	11.5	1.13	15.3		
280	12.60	34.89	26.43	128	18.6	1.45	20.7		
280	···	35.95†	···					−38.3	pump*
283	12.54	34.89	26.44	128	18.6	1.46	20.8		
344	10.60	34.77	26.71	75	26.9	1.98	29.6		0.20 TU
350	···	*34.79*	···					−72.2	pump* no ³H
403	9.40	34.70	26.86	70	31.3	2.16	32.7		
438	8.50	34.64	26.96					−99.0	
462	8.14	34.63	27.00	77	37.3	2.29	34.5		
GEOSECS 331: 4.6°S, 125.1°W									
100	16.59	35.28	25.86	123	7.5	1.27	13.1		
100	···	35.20	···					+22.5	pump*
116	14.51	35.03	26.13	54	16.6	1.88	25.1		
138	13.17	34.95	26.36	34	21.3	2.05	29.7		
178	12.54	34.92	26.46	32	23.8	2.11	30.7		
226	12.13	34.88	26.51	6	27.4	2.31	33.5		0.12 TU
240	···	*34.88*	···					−77.2	pump*
273	11.55	34.85	26.60	19	28.4	2.30	33.0		0.18 TU
302	10.98	34.82	26.68					−92.1	
305	10.98	34.82	26.68	4	32.1	2.46	35.0		0.28 TU
374	9.76	34.76	26.84	29	32.9	2.43	35.3		
GEOSECS 334: 0.1°N, 124.5°W									
110	···	34.84						+47.5	pump*
111	18.93	34.84	24.94	130	11.9	1.07	14.1		
137	14.63	34.75	25.89	125	19.1	1.29	17.7		
160	···	34.92	···					−19.5	pump*
180	13.49	34.75	26.13	130	17.7	1.36	18.7		1.32 TU
195	···	34.92	···					−45.6	pump*
204	12.73	34.92	26.42	121	18.9	1.49	20.9		
282	11.99	34.86	26.52	100	21.8	1.72	24.7		0.46 TU
366	11.08	34.80	26.65	33	28.8	2.18	32.6		0.19 TU
479	8.75	34.67	26.94	24	40.4	2.55	38.1		
GEOSECS 337: 4.8°N, 124.1°W									
122	16.82	34.74	25.39	90	16.3	1.56	21.2		
130	14.76	34.70	25.82					−30.2	
147	13.04	34.66	26.16	74	24.9	1.83	25.4		2.06 TU
167	11.68	34.63	26.40	88	27.9	1.85	25.7		1.41 TU
190	11.16	34.64	26.50					−75.5	
197	10.92	34.63	26.54	91	30.3	1.90	26.5		0.94 TU
225	10.43	34.67	26.66	94	30.2	1.92	27.3		0.58 TU
250	10.09	34.67	26.72					−94.8	
260	9.92	34.67	26.75	75	32.3	2.09	30.3		0.32 TU

Italic entries highlight specific large-volume water samples referred to in the text.

*$\Delta^{14}C$ sample collected by a surface pump connected to a long hose lowered over the ship's side. Depths for pump samples must be viewed with caution, as there are no temperatures for confirmation. Stated depths are especially suspect at the equator, where large angles may develop between the hose and the true vertical due to strong current shear.

†The salinity from the 280-m pump sample at station 246 is reported by *Ostlund et al.* [1987] to be 33.95‰ even though no salinities this high are associated with ~12.5°C temperatures anywhere in the Pacific Ocean.

[*Ostlund et al.*, 1987]. Examining the $\Delta^{14}C$ observations in Table 2 in light of the preceding discussion, one finds three stations in the western South Pacific with $\Delta^{14}C$ levels of $-72\%o$ just below the depth where tritium becomes undetectable: 397 m at station 257, 296 m at station 251, and ~300–350 m at station 246 (see Figure 17 for locations). The fact that there is no tritium in these samples means that their $\Delta^{14}C$ levels have not been affected by bomb ^{14}C. The $-72\%o$ water in the western South Pacific has a temperature of about 11°C and a salinity of about 34.80‰, which puts it right in the deep mode of eastward Equatorial Undercurrent transport identified in Figure 9.

GEOSECS station 331 at 4.6°S, 125.1°W, in the eastern Pacific includes a $\Delta^{14}C$ sample at the southern fringe of the core of the 13° Water according to *Tsuchiya* [1981]. The 240-m sample has a temperature of about 12.1°C, a salinity of 34.88‰, a $\Delta^{14}C$ content of $-77.2\%o$, and only a trace of tritium (~0.15 TU). The 240-m sample is thus slightly warmer and slightly saltier and has a $\Delta^{14}C$ content within measurement error of the 11° tritium-free water in the western South Pacific.

$\Delta^{14}C$ levels of -72 and $-77\%o$ are very similar to the $\Delta^{14}C$ levels inferred for the Peru upwelling from the Galapagos coral. This is probably not a coincidence. Two important water masses in the lower thermocline, one 11°C, the other 12°C, which can be associated hydrographically with the eastward transport in the lower part of the undercurrent, have nearly the same prebomb $\Delta^{14}C$ levels as the water upwelling off Peru (15°–16°C). If one allows for diapycnal mixing between the warm water in the core of the undercurrent and the water below, the 11° water in the western Pacific and the 12°–14° thermostad water in the east can be transformed into the water which is observed to upwell off Peru. Of course, one expects diapycnal warming to be accompanied by a corresponding increase in $\Delta^{14}C$. We will show in the discussion section below that the expected increase for prebomb $\Delta^{14}C$ is very small.

Tsuchiya [1981] shows that the 13° Water extends north of the equator as well as south. However, the variety of 13° Water north of the equator is significantly fresher and much more contaminated with tritium at the time of GEOSECS. At GEOSECS station 337, at 4.8°N, 124°W, one finds a sample at 190 m with a $\Delta^{14}C$ content of $-75.5\%o$. It has a temperature of 11.2°C and a salinity of 34.635‰. It also has a tritium content of about 1 TU. Given the level of tritium contamination, one expects that the prebomb $\Delta^{14}C$ content of northern thermostad water would have been significantly lower, perhaps -85 or $-90\%o$.

In Table 3 we have tabulated some observations from a cross-equatorial transect at 150°W made in 1979 as part of the Hawaii to Tahiti shuttle program (North Pacific Experiment, or NORPAX) [*Quay et al.*, 1983]. These samples were collected 5 years after the GEOSECS samples. The ^{14}C sample density during the NORPAX cruise was much greater relative to GEOSECS. The most interesting feature in this data set, from the standpoint of this paper, is a core of high oxygen found at 234 m at 2.5°S (station 16). Water at 234 m has an oxygen content of 90 μmol kg^{-1}, compared with levels of 40 to 50 μmol kg^{-1} above and below. Given the hydrographic setting [*Tsuchiya*, 1968], it is clear that the high-oxygen core represents a direct infusion of water from the west. The water in the core of high oxygen has a temperature of 11.94°C and a salinity of 34.85‰. The high-

oxygen core sits within a 100-m-thick layer of minimum stability, which suggests that this layer is part of the 13° thermostad, even though it is west of the region where the thermostad is usually defined.

The high oxygen core is also a $\Delta^{14}C$ maximum. $\Delta^{14}C$ levels just above and below the high oxygen core are -51 and $-53\%o$, relative to $-60\%o$ and $-77\%o$ at the top and bottom of the stability minimum, respectively. We suggest that the high-oxygen core at NORPAX 16 represents a recent arrival with a small amount of bomb ^{14}C that was not evident at the time of GEOSECS. If bomb ^{14}C has in fact first appeared in the thermostad between 1974 and 1979, then the transit time for the water to move from its point of last contact with the atmosphere into the Equatorial Undercurrent is about 15 years. Within the lower undercurrent regime there is a substantial amount of recirculation between eastward flowing high-oxygen water close to the equator and westward flowing low-oxygen water between 3° and 8°S [*Tsuchiya*, 1968; *Tsuchiya et al.*, 1990]. To the extent that lower undercurrent water reaching the Galapagos Islands and Peru is a mixture of newly injected and recirculated water, the ventilation age of the water upwelling off Peru could be significantly greater than 15 years.

DEVELOPMENT OF THE EQUATORIAL $\Delta^{14}C$ PROPERTIES IN THE MODEL

One cannot sample the prebomb ocean any longer, except at the surface with corals. However, it is useful to analyze the *Toggweiler et al.* [1989a] model's prebomb $\Delta^{14}C$ simulation for its general properties and to examine the correspondence between prebomb $\Delta^{14}C$ and the measurable properties (i.e., temperature, salinity, and postbomb $\Delta^{14}C$) that characterize the water masses of the equatorial Pacific. It should also prove instructive to review why the model fails to upwell low-$\Delta^{14}C$ water in the right place.

Figure 10 shows a series of north-south sections down the eastern Pacific GEOSECS track, along approximately 125°W, which includes (from the top) temperature, salinity, and 1974 $\Delta^{14}C$. The panels on the right (Figures 10e, 10f, and 10g) were constructed from GEOSECS observations. The panels on the left were constructed from the model and include a prebomb $\Delta^{14}C$ section (Figure 10d, at the bottom). The data-model comparison in Figure 10 does not show off the model at its best. The eastern Pacific section is included here because it cuts through the area of the Pacific where the erroneous surface distributions in Figures 6 and 7 are generated. On the other hand, Figure 10 does suggest that the model does a respectable job of reproducing the larger patterns of the postbomb $\Delta^{14}C$ distribution. To the degree that this is true, one should be able to rely on the model to characterize the general properties of the $\Delta^{14}C$ distribution in prebomb times.

In order to identify the position of the eastward flowing water of the lower Equatorial Undercurrent in the salinity and bomb $\Delta^{14}C$ sections, the 11°–14°C temperature range has been hatched in all three panels of observations (right). The equivalent part of the undercurrent in the model is somewhat warmer, so the 15°–17°C temperature range has been hatched as a reference point in the four panels of model results (left). The model generally succeeds in reproducing the salinities and $\Delta^{14}C$ levels characteristic of the lower part of the undercurrent. In both the model and the observations,

TABLE 3. Equatorial Pacific Hydrographic Data From NORPAX

Depth, m	θ, °C	Salinity, ‰	σ_θ, ‰	Concentration, μmol kg^{-1}				$\Delta^{14}C$, ‰	Comments
				Oxygen	Silica	Phosphate	Nitrate		
NORPAX 13: 5.0°S, 150.0°W (1979)									
188	16.55	35.27	25.85	128	5.9	1.21	13.4	+92.4	
221	14.48	35.05	26.16	87	10.6	1.66	19.2		
221	13.01	34.93	26.38	54	16.0	1.99	24.3	−16.4	
255	11.15	34.82	26.65	24	26.7	2.38	31.8	−72.1	
321	9.99	34.76	26.80	32	30.9	2.43	33.6	−86.6	
387	9.04	34.70	26.92	45	33.8	2.44	34.5		
NORPAX 16: 2.5°S, 150.0°W (1979)									
131	16.11	35.28	25.97	104	9.0	1.48	18.4		
133	14.56	35.09	26.17	···	15.2	1.88	25.2	+6.7	
141	14.14	35.05	26.23	61	16.3	1.95	26.5		
159	13.12	34.96	26.37	···	20.7	2.12	29.8	−43.2	
172	12.67	34.92	26.43	40	22.7	2.19	31.0		
193	12.34	34.89	26.48	···	24.5	2.24	31.8	−59.9	stab.min*
203	12.22	34.88	26.49	49	23.8	2.16	30.5		stab.min*
227	11.97	34.85	26.52	···	22.6	1.90	26.7	−50.9	stab.min*
234	11.94	34.85	26.52	90	22.6	1.91	26.9		stab.min*
261	11.78	34.84	26.55	···	23.4	1.95	27.8	−53.0	stab.min*
291	11.62	34.85	26.58	55	25.2	2.17	30.7		stab.min*
294	11.49	34.84	26.60	···	26.2	2.25	31.6	−76.8	
334	10.87	34.81	26.69	···	29.7	2.44	33.7	−86.0	
373	10.24	34.77	26.77	26	32.9	2.56	35.5		
535	7.47	34.61	27.08	···	44.9	2.69	37.9	−124.6	
NORPAX 21: 0.0°N, 150.0°W (1979)									
157	16.73	25.24	25.79	148	9.2	1.01	13.7		
171	15.15	35.11	26.05	145	12.3	1.12	15.9	+17.9	
195	13.31	34.96	26.33	133	16.8	1.35	19.6	−15.6	
224	12.60	34.90	26.43	124	19.2	1.47	21.7	−32.9	
261	11.57	34.83	26.58	72	25.0	1.88	28.4	−60.3	
310	10.52	34.77	26.72	51	30.0	2.13	32.6	−71.7	
353	9.97	34.73	26.78	52	31.9	2.17	32.8	−85.9	
426	8.58	34.65	26.95	63	36.9	2.29	34.9		
NORPAX 25: 2.0°N, 150.0°W (1979)									
121	13.98	34.71	26.00	110	22.0	1.49	21.7	+3.0	
132	12.88	34.69	26.21	97	23.8	1.58	23.3		
135	12.74	34.72	26.27	103	24.1	1.63	24.0	−24.2	
149	12.15	34.76	26.41	92	25.0	1.74	26.0	−42.0	
169	11.72	34.83	26.55	68	25.7	1.91	28.8	−59.8	
233	11.33	34.81	26.60	66	26.4	1.95	29.7	−67.7	
334	10.43	34.74	26.71	66	29.5	2.05	31.1		
389	8.87	34.65	26.90	50	40.6	2.40	36.4	−110.3	

*Layer of minimum stability containing high oxygen, high $\Delta^{14}C$ core.

salinities in the hatched regions are between 34.8 and 35.0‰. Thermostad water at the time of GEOSECS had a $\Delta^{14}C$ content of roughly −40 to −80‰. The model's 15°–17° water has very similar $\Delta^{14}C$ levels 11 years after the bomb tests. The model predicts a prebomb $\Delta^{14}C$ content of −65 to −80‰ in the hatched region. Just above the hatched regions in the model, one sees a strong penetration of low-salinity water from the north and a strong penetration of high-salinity water from the south. These features are not apparent in the observations. This discrepancy will be examined in more detail in the figures that follow.

The increase in atmospheric $\Delta^{14}C$ following the bomb tests changed the radiocarbon tracer from being a weakly forced tracer to a rather strongly forced tracer. This change is illustrated very clearly by the differences between the prebomb $\Delta^{14}C$ section in Figure 10d and the postbomb Figures 10c and 10f just above. Many contour lines are bunched together in the upper 300 m of the postbomb plots, whereas prebomb contours are particularly sparse in the

upper 300 m. Because the equilibration time for $^{14}C/^{12}C$ ratios at the surface is so slow, the recirculation of tropical and subtropical water through the shallow equatorial upwelling system acts to homogenize upper ocean $\Delta^{14}C$ levels under prebomb conditions. Water moves from region to region and changes temperature faster than ^{14}C can come in from the atmosphere. Under postbomb conditions the input of ^{14}C to the ocean increases by a factor of 10. Upper ocean layers with the most frequent contact with the atmosphere become loaded with bomb ^{14}C. Gradually the less well ventilated layers begin to fill up with bomb ^{14}C, until the upper ocean $\Delta^{14}C$ distribution acquires large upper ocean gradients.

Figure 11 shows a longitude by depth section across the model Pacific basin at 6.75°S. Figure 11 illustrates how the prebomb and postbomb tracers label distinctly different water masses in the tropical Pacific. In Figure 11a, prebomb $\Delta^{14}C$ contours are overlaid on the model temperature field. In Figure 11b the most bomb-contaminated part of the $\Delta^{14}C$
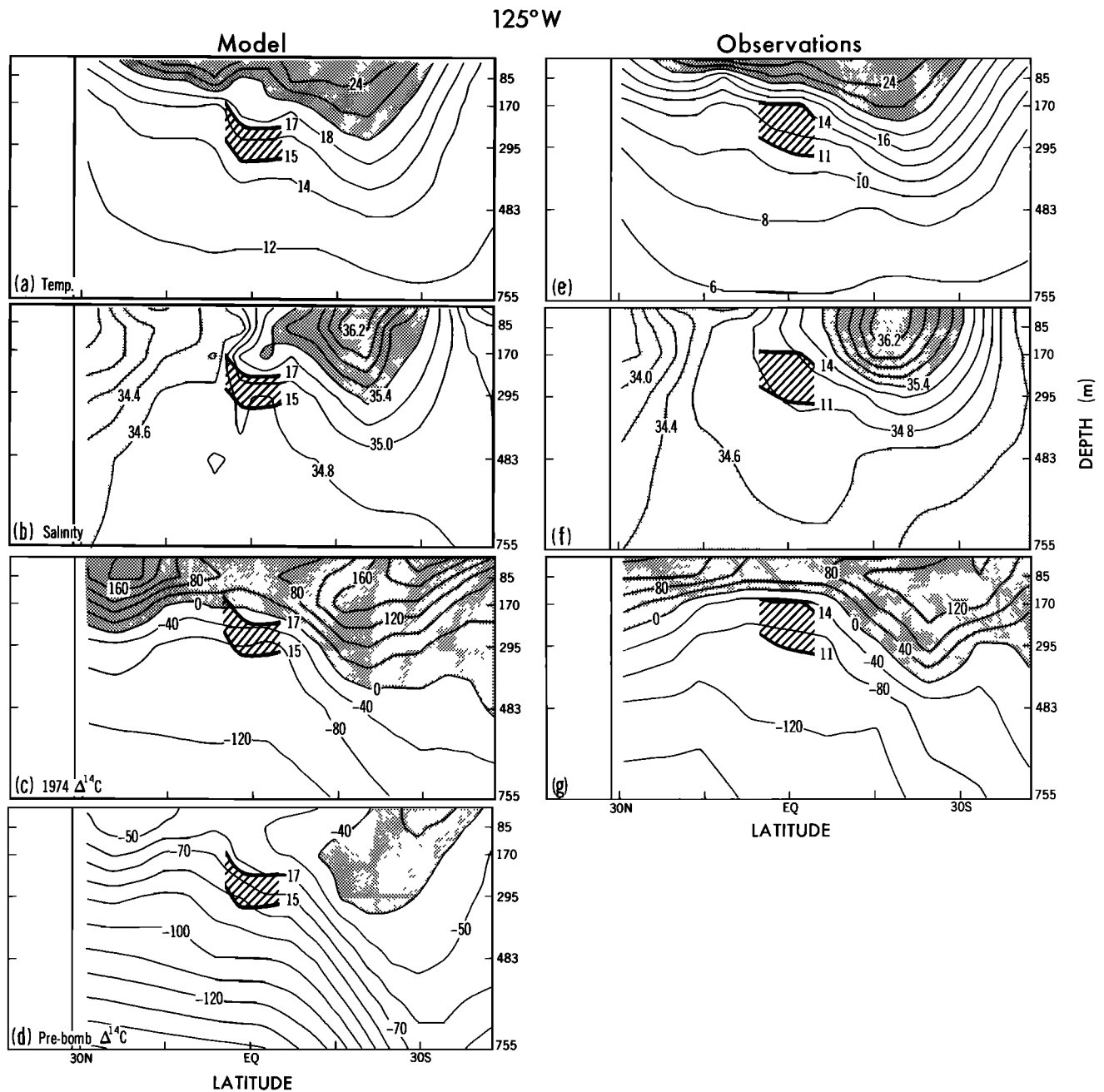
125°W

Fig. 10. Comparisons between observed and modeled water properties along the east Pacific GEOSECS track (~125°W). Panels on the left show model sections for (a) temperature, (b) salinity, (c) 1974 Δ^{14}C, and (d) prebomb Δ^{14}C [*Toggweiler et al.*, 1989a, b]. Panels on the right show (e) temperature, (f) salinity and (g) 1974 Δ^{14}C as observed during GEOSECS [*Broecker et al.*, 1982; *Ostlund et al.*, 1987].

field is contoured over the salinity field. The flow across this section is southward away from the equator in the surface layer and equatorward below. The strongest equatorward flow by far is found in the center of the basin in the second layer (85 m).

The model produces a Δ^{14}C maximum (+120‰) which advects toward the equator in the center of the basin between 150°W and the date line. The bomb Δ^{14}C maximum is closely aligned with a salinity maximum on level 3 (170 m). In this case, the model's configuration fits very well with the Δ^{14}C and salinity observations in *Quay et al.* [1983]. The bomb Δ^{14}C and salinity maxima are associated with subtropical water which is about 22°–24°C. As such they sit at the

base of the layer feeding the equatorial divergence from the south. The most vigorously upwelled water lies just above in layer 2. It is much less distinct with regard to Δ^{14}C and salinity because it is repeatedly overturned by the upwelling system within 10° of the equator. Figure 11a shows that the prebomb Δ^{14}C content of water warmer than 22°C is relatively invariant with temperature, in contrast with the layers below. The upwelling of subtropical water, which leaves such a distinct imprint on the subsurface distributions of bomb ^{14}C and salinity, has virtually no effect on the prebomb distribution.

Figure 6 showed that the model produces a prebomb Δ^{14}C minimum on the equator near 120°W. Figure 12 illustrates
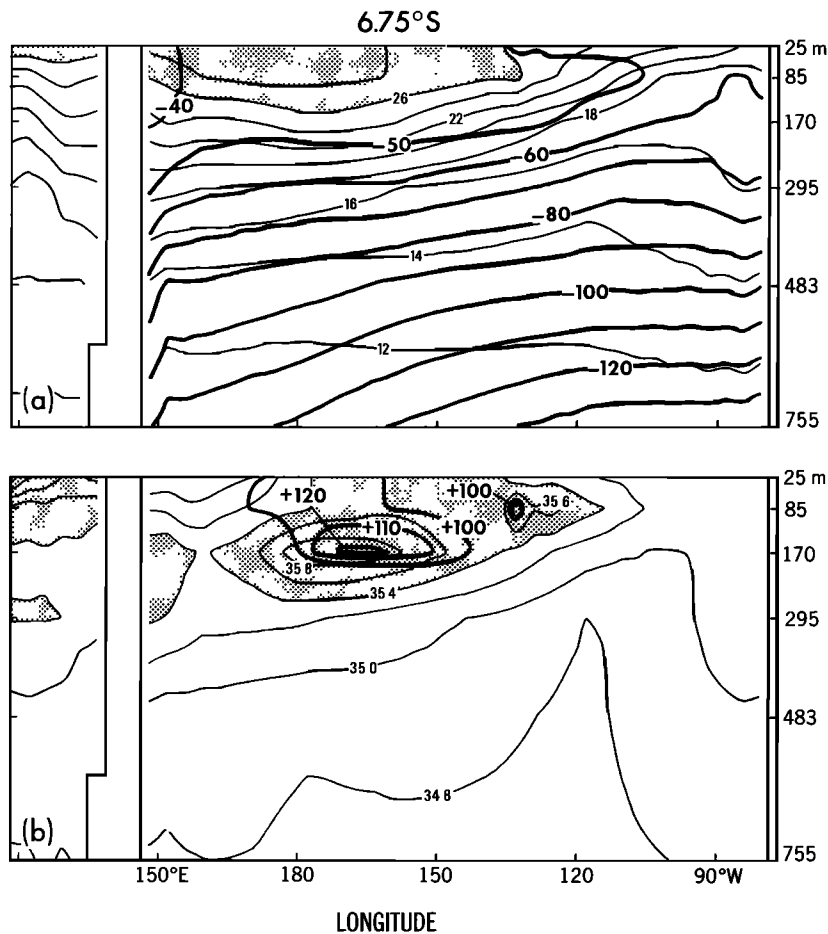
6.75°S

Fig. 11. (a) Model results showing the correspondence between prebomb $\Delta^{14}C$ (bold contours) and temperature along an east-west section at 6.75°S. (b) Model results showing the correspondence between postbomb $\Delta^{14}C$ (1974) and salinity along 6.75°S. Only $\Delta^{14}C$ levels greater than +100‰ are contoured. Model results are from Toggweiler et al. [1989a, b].

how the model's $\Delta^{14}C$ minimum develops from the circulation field. Figure 12a shows the prebomb $\Delta^{14}C$ distribution on level 2 of the model (85 m) in the eastern tropical Pacific. Figure 12b shows model current vectors for the same layer. Level 2 has a distinct $\Delta^{14}C$ minimum (<−65‰) 5° to 10° north of the equator along 105°W. The flow along the southern and western edge of the $\Delta^{14}C$ minimum carries low-$\Delta^{14}C$ water toward the equator where it joins up with the model's Equatorial Undercurrent and upwells to the surface.

The upward doming of $\Delta^{14}C$ isopleths near 10°N in the eastern tropical Pacific is not unlike what happens to isopleths of density in this sector of the real ocean. However, the direct advection of the low-$\Delta^{14}C$ water toward the equator in this sector is not realistic. Figure 13 shows a comparison of observed and modeled salinities at the depth of layer 3 in the model (170 m). In the model, a tongue of low salinity water (<34.4‰) projects strongly toward the equator from the north in the east central sector of the Pacific. No feature like this is present in the observations. The low-salinity tongue from the north is not exactly analogous to the model's low-$\Delta^{14}C$ feature in Figure 12, since it follows a path toward the equator from much higher latitudes. Nevertheless, both features appear to be totally spurious, in the sense that both features project all the way to the equator and become incorporated into the equatorial upwelling. South of

the equator, a high-salinity tongue penetrates to the equator between 180°E and 150°W, while a second low-salinity tongue penetrates toward the equator near South America. Neither feature is evident in the observations.

One consequence of the model's coarse resolution is the fact that maximum current speeds are often too weak. Nowhere is this more true than in the case of the Equatorial Undercurrent. The maximum current speed for the model undercurrent is only about 15–20 cm s^{-1}, when more than 100 cm s^{-1} is expected [Wyrtki et al., 1981]. Since the undercurrent is not directly forced by the wind, its speed and flow volume are greatly attenuated by the viscosity introduced into the model to maintain numerical stability. Because the undercurrent in the model is so weak, much less high-salinity water is fed into the equatorial region from the south along the western margin as in the observations of Lindstrom et al. [1987] and Tsuchiya et al. [1990]. Nearly all the water feeding the core of the undercurrent in the model is locally derived in the central and eastern sectors of the basin. It is this excessive local convergence of subsurface water that accounts for the spurious tongues of low and high salinity in Figures 10 and 13.

The model's northern hemisphere $\Delta^{14}C$ minimum in Figure 12 is connected to a more pronounced minimum on level 3 which is centered between 10° and 15°N in a broad zone of weak upwelling off Central America. The $\Delta^{14}C$ minimum on
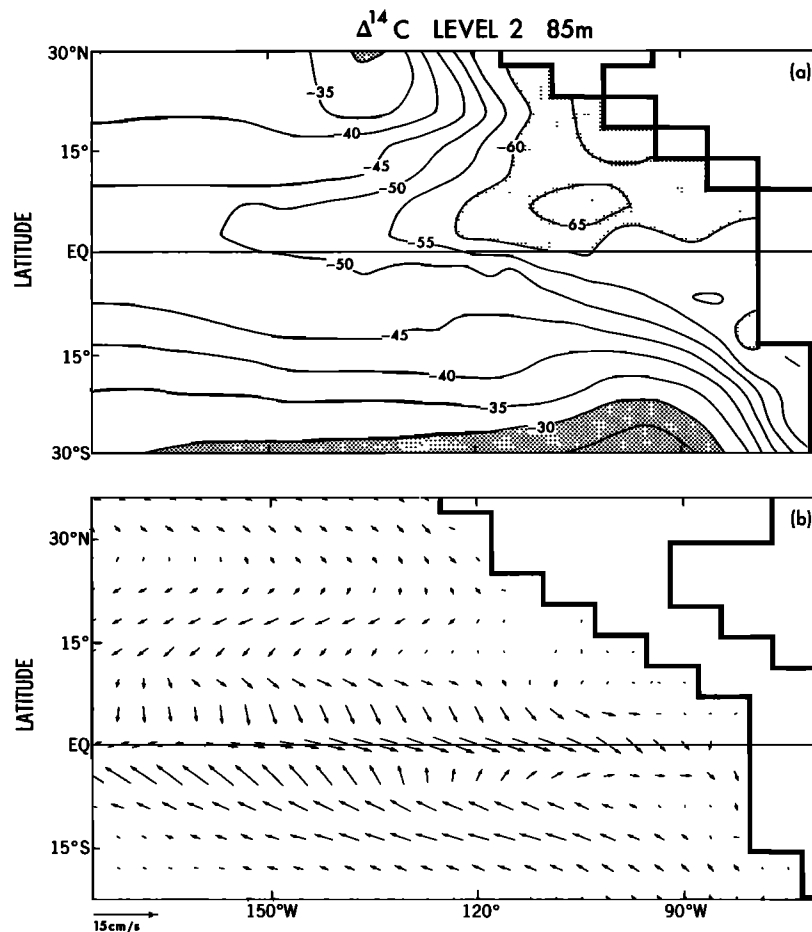
Δ^{14}C   LEVEL 2   85m

Fig. 12.   (a) Prebomb distribution of Δ^{14}C on level 2 (85 m) of the *Toggweiler et al.* [1989a] model in the eastern tropical Pacific. (b) Model current vectors at the same depth, showing how low-Δ^{14}C water from the north becomes incorporated into the equatorial upwelling.

level 3 extends to many levels below. It owes its origin to the upwelling of abyssal water which entered the Pacific basin as bottom water flowing north from the Antarctic. Thus the model's Δ^{14}C minimum along the equator is part of the closure of its deep thermohaline circulation which is initiated by deep water formation in high latitudes.

Discussion

High-Latitude Origin of the Peruvian Upwelling

In searching for the origin of the 13° Water in the Equatorial Undercurrent, *Tsuchiya* [1981] mapped the basin-wide properties of a density surface which bisects the 13° thermostad in the undercurrent ($\sigma_\theta \approx 26.45$). He concluded that winter convection or vertical mixing in the Tasman Sea or in the region northeast of New Zealand produces a subsurface water mass that flows around the South Pacific subtropical gyre and up to the equator, where it becomes incorporated into the undercurrent. According to Tsuchiya's isopycnal analysis, the source water for the thermostad is found between 35° and 40°S and has a temperature of 14°C and a salinity of about 35.2‰.

Tsuchiya's analysis puts the origin of the water in the lower part of the undercurrent at the southern fringe of the South Pacific subtropical gyre. This conclusion is not consistent with the Δ^{14}C content of the water. In Figure 14 we

show a map of prebomb surface Δ^{14}C levels predicted by the *Toggweiler et al.* [1989a] model for the western South Pacific. The transect of stations which Tsuchiya used to construct his proposed flow path for the 13°C Water has been overlaid on the Δ^{14}C map. The area near the southeast coast of Australia claimed by Tsuchiya as the source of the 13° Water has been indicated on the figure. The model predicts a prebomb Δ^{14}C content of only -45 to $-50‰$ in this region. According to the model, surface waters in the latitude belt of northern New Zealand do not have Δ^{14}C levels nearly low enough to account for the Δ^{14}C in the 13°C Water or in the prebomb growth bands of the Galapagos coral. According to the model, one must look to surface water 10° or so further south to find the appropriate levels of radiocarbon.

No corals grow south of 30°S in the South Pacific to allow us to recover Δ^{14}C levels that truly predate the bomb effect. There were, however, a number of seawater samples collected for radiocarbon analysis by New Zealand and American geochemists in late 1957 and early 1958 which help confirm the model's representation of the prebomb Δ^{14}C field in the middle and high latitudes of the South Pacific. The surface water data from *Rafter* [1968] and *Bien et al.* [1965] are reproduced here as Table 4.

Figure 15 shows a scatter plot of the model's prebomb Δ^{14}C points in Figure 14 replotted as a function of surface temperature along with the data from Table 4. When plotted

Salinity 170m
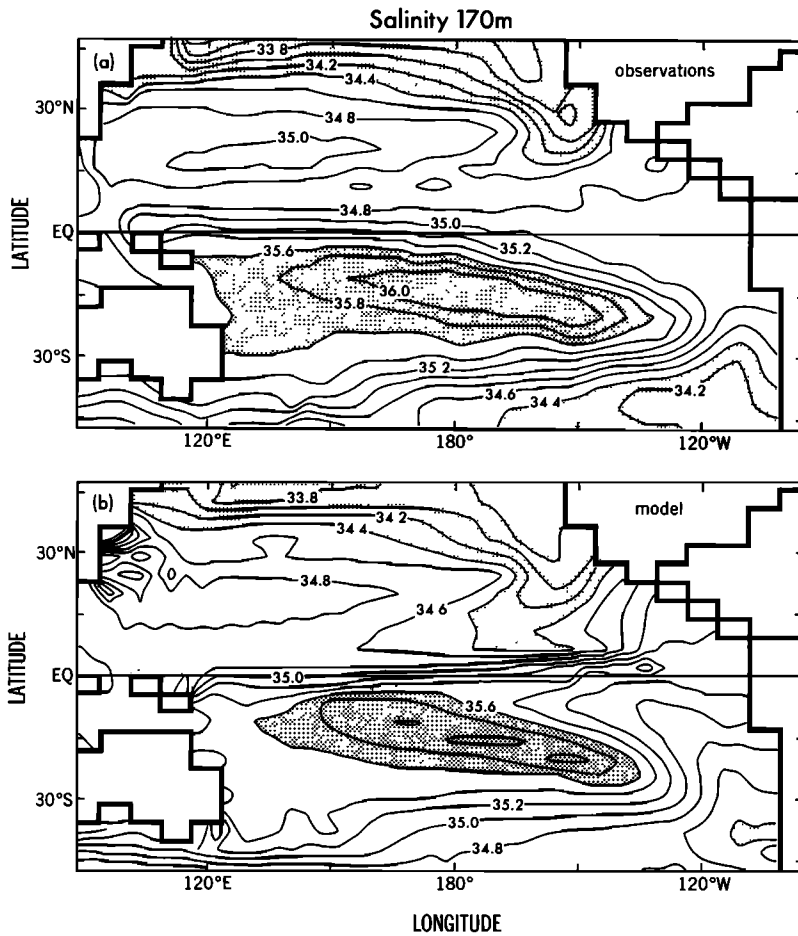
Fig. 13. Comparison between (top) observed and (bottom) modeled salinities on level 3 (170 m) in the *Toggweiler et al.* [1989a, b] model. Observed salinities have been interpolated from the *Levitus* [1982] data set to the model grid.

Surface Δ¹⁴ C – prebomb
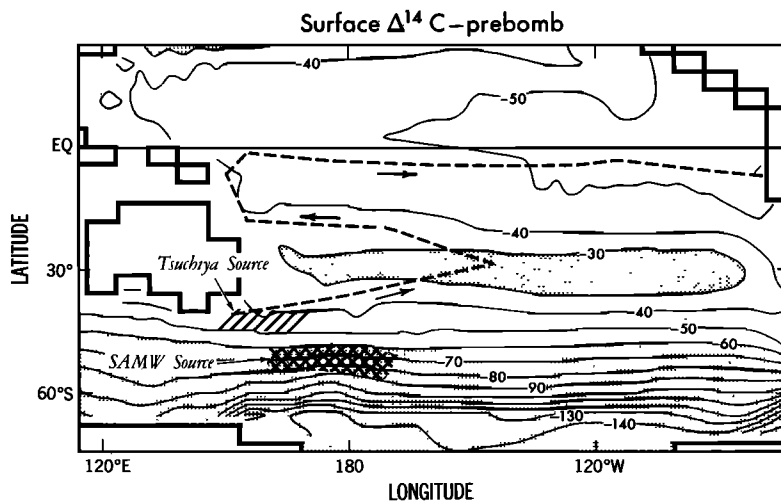
Fig. 14. Flow path of the equatorial 13° Water from its outcrop position southeast of Australia (slant-hatched region) into the Equatorial Undercurrent, according to the isopycnal analysis of *Tsuchiya* [1981]. Tsuchiya's flow path has been overlaid on the prebomb surface $\Delta^{14}C$ distribution from the *Toggweiler et al.* [1989a] model. According to the model, Tsuchiya's source region for the 13°C Water has a prebomb $\Delta^{14}C$ of only -40 to $-50‰$ and cannot be the source of the -70 to $-80‰$ water observed in the undercurrent. The 13°C Water must originate further south, in the latitude belt where Subantarctic Mode Water (SAMW) forms (cross-hatched region).

TABLE 4. $\Delta^{14}C$ Measurements Made on South Pacific Surface Seawater Samples Collected by March 1958

Sample No.	Latitude	Longitude	Collection Date	T, °C	S, ‰	$\Delta^{14}C$, ‰
New Zealand Measurements Reported by Rafter [1968]						
A.409	15.2°S	179.1°W	March 1958	30	⋯	−41 ± 6
A.514	18.3°S	172.3°W	March 1958	29	⋯	−43 ± 3
A.404	20.9°S	175.4°W	March 1958	27	⋯	−36 ± 9
A.513	21.3°S	177.5°W	March 1958	28	⋯	−40 ± 6
A.407	21.3°S	173.3°W	March 1958	28	⋯	−38 ± 5
A.512	28.8°S	176.0°E	March 1958	22	⋯	−42 ± 6
A.515	32.9°S	175.8°E	March 1958	23	⋯	−43 ± 6
A.511	36.6°S	174.9°E	March 1958	23	⋯	−50 ± 9
A.344	37.4°S	170.6°E	March 1958	21	⋯	−58 ± 5
NZSS*	41.1°S	178.0°E	Nov. 1954 to March 1958†	16.0	⋯	−47 ± 4†
A.395	46.2°S	171.2°E	Feb. 1958	12	⋯	−63 ± 8
A.394	51.5°S	169.1°E	Feb. 1958	11	⋯	−70 ± 5
A.392	59.9°S	169.6°E	Feb. 1958	7	⋯	−91 ± 4
A.357	66.5°S	164.0°E	Feb. 1958	1	⋯	−128 ± 3
Measurements Reported by Bien et al. [1965]						
LJ68	34.8°S	135.9°W	Nov. 1957	17.7	35.05	−38 ± 8
LJ93	42.7°S	96.0°W	Dec. 1957	11.5	⋯	−40 ± 8
LJ90	46.5°S	116.0°W	Dec. 1957	9.2	34.67	−60 ± 8

*New Zealand Standard Station.
†Average of eight measurements.

against temperature, model $\Delta^{14}C$ surface levels show a distinct break at about 14°C (40°–45°S). The $\Delta^{14}C$ content of surface water colder than 14°C decreases quite steeply with decreasing temperature, whereas the $\Delta^{14}C$ content of surface water warmer than 14°C is relatively invariant with respect to temperature. The data points in Figure 15 suggest that the model captures these trends quite well.

The break in the $\Delta^{14}C$ trend with temperature at about 14°C marks the Subtropical Convergence (STC) in the South

Pacific. South of 40°S surface $\Delta^{14}C$ levels are very low owing to the upwelling of cold, low-$\Delta^{14}C$ abyssal water around Antarctica and the northward drift of the Antarctic water under the circumpolar westerlies [Deacon, 1937]. The STC denotes the limit to which Antarctic water is transported northward before downwelling north of the Antarctic Circumpolar Current. The −70 to −75‰ $\Delta^{14}C$ levels observed in the lower undercurrent and the Galapagos coral require that the source for this water must lie south of the STC in the zone influenced by Antarctic water. Surface water with an appropriate $\Delta^{14}C$ level has a temperature of about 8°C. This is much colder than the 14°C source proposed by Tsuchiya [1981].

The method used by Tsuchiya to trace the flow path in
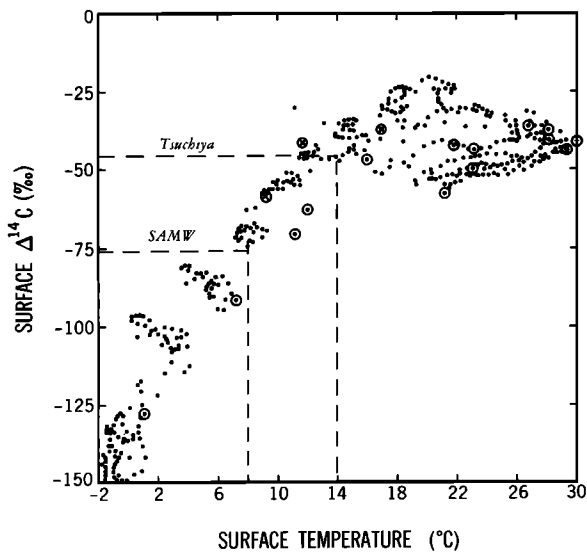
Fig. 15. Prebomb South Pacific surface $\Delta^{14}C$ levels predicted by the Toggweiler et al. [1989a] model (Figure 14) replotted as a function of surface temperature along with prebomb South Pacific $\Delta^{14}C$ seawater observations (Table 4). Data sources are Rafter [1968] (open circles) and Bien et al. [1965], (crossed circles). The observations serve to verify that the source for the 13°C Water in the undercurrent and the Peru upwelling must lie in the region south of the Subtropical Convergence, where surface waters are colder than 14°C.
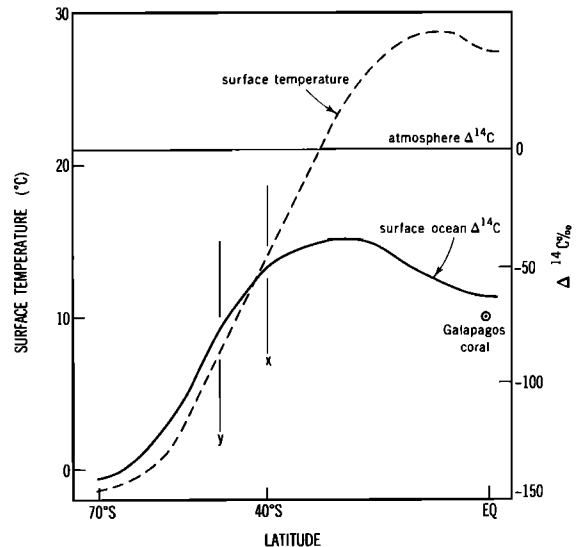
Fig. 16. Schematic diagram showing the variation in surface temperature and prebomb $\Delta^{14}C$ with latitude. The diagram contrasts the time scale of atmospheric forcing on each tracer (see text).
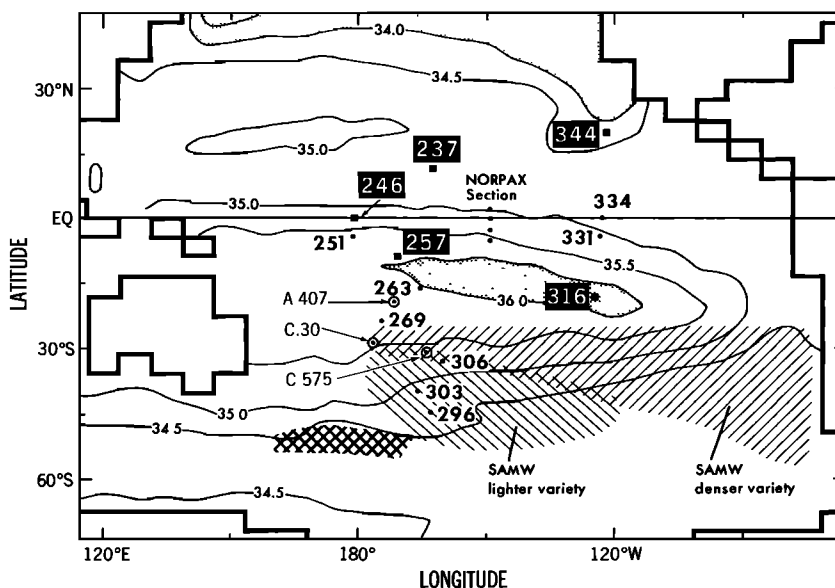
Fig. 17. Map showing the locations of stations appearing in Tables 2, 3, 5, and 6 and in Figures 18 and 19. Station locations are overlaid on the observed salinity distribution at 170 m [*Levitus*, 1982]. The GEOSECS stations used in constructing Figure 18 are indicated by the north-south transect of plain boldface numbers between 170 and 180°W. The locations of stations used in Figure 19 are given by white-on-black numbers. The New Zealand stations in Table 6 are indicated by lightface numbers. The map also shows areas of the South Pacific where *McCartney* [1982] has identified the lighter and heavier varieties of SAMW.

Figure 14 assumes that diapycnal mixing, i.e., mixing normal to isopycnal surfaces, is unimportant with respect to mixing and flow along isopycnals. This is an assumption that is often made because the effect of diapycnal mixing is thought to be very small in thermocline water masses ventilated over time scales of a decade or less [*Jenkins*, 1987]. While we do not claim to have any special knowledge concerning appropriate levels of diapycnal mixing in the South Pacific, there is evidence (presented earlier) suggesting that the time scale for ventilation of the water masses in the lower part of the undercurrent is longer than 15 years. It is quite possible that a strictly isopycnal analysis of the sources of the water in the lower part of the undercurrent pushes the assumption of zero diapycnal mixing beyond its useful limit.

A thermocline water mass's initial prebomb Δ^{14}C content should be much less sensitive to the effect of diapycnal mixing than its initial temperature or density would be. Figure 16 shows schematically the latitudinal distributions of temperature and prebomb Δ^{14}C in the South Pacific in order to contrast the ways in which these tracers respond to external forcing at the air-sea boundary. When averaged over the seasonal cycle, air temperatures over the ocean are within 1° of ocean surface temperatures [*Oort*, 1983]. This close coupling reflects a relatively short time scale for air-sea heat exchange. Sea surface temperatures rise sharply north of 40°S reflecting the input of heat in the tropics and subtropics. Oceanic Δ^{14}C levels, on the other hand, are quite independent of atmospheric Δ^{14}C levels and mainly reflect latitudinal differences in the extent of contact between surface waters and low-Δ^{14}C deep water. Most significantly, prebomb Δ^{14}C levels north of 40°S are relatively flat, reflecting the weak input of ^{14}C from the atmosphere and the extensive recirculation of a small amount of upwelled low-Δ^{14}C water throughout the tropics and subtropics.

The ocean's thermocline is made up of progressively

cooler layers which have been subducted into the interior from progressively higher latitudes. If a surface water mass from the latitude marked x in Figure 16 (approximately the latitude of *Tsuchiya*'s [1981] high-latitude source for the 13° Water) is moved northward below water masses forming at lower latitudes, it will be significantly cooler than all the overlying water, but it will have virtually the same Δ^{14}C content as the overlying water. Thus, water from x might be warmed by mixing, but its Δ^{14}C content cannot change. At the same time it cannot be the source for the upwelled water off Peru, because its initial Δ^{14}C content is too young. On the other hand, an 8°C water mass from the latitude marked y starts off with a Δ^{14}C content a bit lower than that of the Peru Upwelling. The Δ^{14}C gradient in the overlying water is still quite small. Given some mixing, the temperature of the y water mass may rise a few degrees while the initial Δ^{14}C increases by a few per mil. In this way it is possible for 8°C water to be transformed into 13° water while it retains a "memory" of its initial Δ^{14}C. The degree to which temperature and Δ^{14}C are altered in this example must be considered in terms of how well each can be measured: a 5° change in temperature represents a dynamic range of at least 1000 in terms of temperature measurement precision, whereas a 10‰ change in Δ^{14}C represents a dynamic range of about 3 in terms of GEOSECS Δ^{14}C precision.

There are several possible ways this analysis could be wrong. First of all, one might want to know whether ^{14}C decay during the trip to the equator could be a factor in this analysis. For a water mass with an initial Δ^{14}C content of -45 to $-50‰$ to acquire a ^{14}C content of -70 to $-75‰$ by decay would require a transit time of about 200 years. Given the time scales being discussed here, ^{14}C decay should not account for more than a 2–4‰ change in thermocline Δ^{14}C levels. Northern hemisphere water with the same density as 13° Water appears to be lower in prebomb Δ^{14}C than

TABLE 5.   South Pacific Hydrographic Data From GEOSECS Covering the Density Range of Subantarctic Mode Water

Depth, m	θ, °C	Salinity, ‰	σθ, ‰	Oxygen	Silica	Phosphate	Nitrate	Δ14C, ‰	Comments
					GEOSECS 296: 45.0°S, 166.7°W				
82	11.46	34.94	26.68	244	3.9	0.76	9.6		
99	11.39	34.96	26.71					+50.4	
152	10.19	34.80	26.80	244	4.1	0.92	12.3		light SAMW
200	9.87	34.76	26.83					+47.6	light SAMW
242	9.53	34.72	26.85	251	4.2	0.99	13.1		light SAMW
375	8.56	34.60	26.91	232	6.6	1.25	17.8		light SAMW
400	8.44	34.58	26.92					+9.8	light SAMW
449	8.00	34.53	26.94	237	7.2	1.34	19.2		light SAMW
548	7.56	34.49	26.98	230	8.6	1.46	21.0		dense SAMW
601	7.59	34.50	26.99					−56.9	dense SAMW
647	7.33	34.49	27.01	216	11.5	1.57	23.0		dense SAMW
745	6.72	34.43	27.05	223	13.3	1.64	24.0		dense SAMW
803	6.44	34.42	27.08					−81.4	
843	6.26	34.42	27.10	211	18.0	1.74	26.1		
941	5.66	34.40	27.16	207	23.7	1.85	27.9		
1002	5.29	34.37	27.18					−92.9	
1040	5.19	34.40	27.22	197	30.3	1.96	29.5		
					GEOSECS 303: 38.3°S, 170.1°W				
151	11.95	35.04	26.67	241	5.0	0.66	8.0		
201	11.47	34.98	26.71	238	5.2	0.74	9.5		
201	11.39	34.97	26.72					+63.3	
250	10.96	34.90	26.75	234	5.4	0.83	10.9		
300	10.50	34.85	26.78	230	5.9	0.89	12.4		light SAMW
351	9.94	34.77	26.83					+21.3	light SAMW
399	9.37	34.69	26.86	231	6.6	1.08	15.1		light SAMW
497	8.52	34.59	26.92	225	7.3	1.28	18.6		light SAMW
501	8.47	34.59	26.92					−8.0	light SAMW
597	7.70	34.50	26.97	229	8.3	1.40	20.6		dense SAMW
696	7.24	34.45	26.99	231	9.1	1.48	21.9		dense SAMW
702	7.12	34.45	27.01					−53.3	dense SAMW
794	6.86	34.43	27.03	224	11.2	1.57	23.4		dense SAMW
892	6.40	34.40	27.07	219	14.9	1.63	24.9		
898	6.16	34.40	27.10					−85.6	
991	5.99	34.39	27.11	212	18.8	1.75	26.6		
1088	5.30	34.39	27.19	200	27.9	1.92	29.0		
1097	5.11	34.39	27.22					−111.0	
					GEOSECS 306: 32.8°S, 163.6°W				
239	11.96	35.04	26.67	220	4.3	0.80	10.4		
287	11.20	34.93	26.73	217	5.3	0.92	12.2		
302	11.00	34.91	26.75					+21.4	
333	10.49	34.83	26.77	214	5.7	1.01	14.2		light SAMW
416	8.91	34.65	26.90	213	6.5	1.27	18.2		light SAMW
454	8.69	34.61	26.90					−32.3	light SAMW
496	7.99	34.53	26.95	224	6.8	1.37	20.0		light SAMW
565	7.41	34.47	26.98	230	7.5	1.44	21.0		dense SAMW
602	7.24	34.46	27.00					−60.4	dense SAMW
645	6.96	34.43	27.02	229	8.7	1.54	22.6		dense SAMW
714	6.63	34.40	27.04	228	9.5	···	···		dense SAMW
787	6.19	34.37	27.07	227	13.5	1.68	25.1		
799	6.27	34.38	27.07					−91.4	
886	5.67	34.37	27.14	213	19.8	1.85	27.6		
999	5.04	34.36	27.21					−105.8	
1012	4.86	34.36	27.22	203	28.6	2.01	29.9		
					GEOSECS 269: 24.0°S, 174.5°W				
355	16.26	35.47	26.08	197	2.1	0.49	6.0		
454	13.31	35.14	26.47	195	2.8	0.75	10.2		
456	13.12	35.10	26.48					+8.3	
554	10.41	34.77	27.74	194	5.4	1.11	16.3		
559	10.47	34.79	26.74					−29.5	
653	7.71	34.47	26.95	206	8.7	1.45	22.4		
753	6.56	34.38	27.03	216	10.9	1.61	25.0		
758	6.46	34.38	27.04					−84.0	
861	5.64	34.34	27.12	208	18.2	1.80	28.1		
863	5.59	34.34	27.13					−99.7	
998	4.78	34.36	27.23	184	33.0	2.04	32.0		

TABLE 5. (continued)

Depth, m	θ, °C	Salinity, ‰	σ_θ, ‰	Concentration, μmol kg^{-1}				$\Delta^{14}C$, ‰	Comments
				Oxygen	Silica	Phosphate	Nitrate		
GEOSECS 263: 16.7°S, 167.1°W									
303	17.68	35.41	25.69	173	2.1	0.62	6.3		
348	15.49	35.14	26.00					+7.5	
431	11.27	34.72	26.55	149	10.5	1.40	18.6		0.20 TU
474	9.98	34.63	26.70					−66.7	
510	8.22	34.51	26.90	158	16.3	1.75	25.1		no ^{3}H
588	6.37	34.37	27.05	207	13.6	1.73	25.8		
599	6.40	34.37	27.05					−85.3	
669	5.75	34.38	27.14	180	26.3	1.99	29.6		
748	5.12	34.41	27.24	164	38.4	2.16	32.3		
798	4.85	34.43	27.28					−135.9	

southern hemisphere water. Thus lateral mixing with northern hemisphere water has the potential to lower the $\Delta^{14}C$ content of the upwelled water in much the same way that Tsuchiya [1981] suggested that mixing might lower the salinity of 13° Water. Tsuchiya et al. [1990], however, reports that the undercurrent in the western Pacific consists of virtually all southern hemisphere water. While it is possible for northern hemisphere water to become incorporated into the lower undercurrent as it moves to the east, T-S relationships (below) suggest that this does not happen.

The $\Delta^{14}C$ Content and T-S Evolution of Subantarctic Mode Water

According to the Toggweiler et al. [1989a, b] model and the limited prebomb ^{14}C data set in Figure 15, water with a $\Delta^{14}C$ content low enough to account for the −70 to −75‰ water in the Equatorial Undercurrent and the Galapagos coral has an initial temperature of about 8°C. If the 8°C temperature is correct, then thermostad water in the equatorial thermocline and the water upwelling off Peru most likely originates as Subantarctic Mode Water [McCartney, 1977, 1982].

Subantarctic Mode Water (SAMW) is an actively ventilated layer of the lower thermocline which is formed along the northern edge of the Antarctic Circumpolar Current (ACC). Mode waters form by the forced injection of mass into a layer of a particular density. In the latitude belt where the SAMW forms, the curl of the wind stress forces surface water downward, preconditioning the water column for deep convection during the winter. Winter convection creates a layer of weak stratification which persists after the upper part of the layer is capped off in the spring.

Using potential vorticity (PV) as a tracer, McCartney [1982] identified two varieties of SAMW in the South Pacific, one slightly more dense than the other, which appear to form in different sectors of the circumpolar belt. The heavier variety of SAMW coincides in density with the salinity minimum in the eastern South Pacific. The lighter variety of SAMW sits above the salinity minimum. In Figures 14 and 17 we have cross-hatched the area in the western South Pacific where the lighter variety of SAMW (~7°-10°C) is thought to form. McCartney's [1982] Figure 1 shows the lighter variety of SAMW following an anticyclonic trajectory as it penetrates the thermocline. This is a very similar trajectory to the one proposed by Tsuchiya [1981] (Figure 14) except for the fact that it is 10° further south.

In this section we attempt to show what SAMW looks like in terms of $\Delta^{14}C$, both during GEOSECS and during pre-bomb time. In Table 5 a listing is compiled of South Pacific GEOSECS data for the density range containing SAMW, following the format of Tables 2 and 3. In Table 6 we reproduce information on three prebomb, subsurface New Zealand $\Delta^{14}C$ samples from Rafter [1968], which were collected within the density range encompassing SAMW. The hydrographic data which accompanies Rafter's $\Delta^{14}C$ measurements is very marginal by modern standards. Rafter does not give salinities for these samples, only temperature and depth. Temperatures are only specified to the nearest degree. Adjacent GEOSECS stations have been used to determine the approximate salinity and density of these samples.

Figure 17 shows the locations of GEOSECS and New Zealand stations used in this analysis. Station locations have been overlaid on a map of salinity at a depth of 170 m. In the middle latitudes of Figure 17 are shown the areas where McCartney [1982] mapped the lighter and heavier varieties of SAMW on the basis of potential vorticity. Four of the GEOSECS stations in Table 5 and two of the New Zealand stations lie within the region identified by McCartney as containing SAMW.

Figure 18 shows a north-south section of $\Delta^{14}C$ plotted against density (σ_θ) following the line of GEOSECS stations in Figure 17 from station 296 (45°S) to station 251 (4.5°S). The GEOSECS $\Delta^{14}C$ data at these stations are given as boldface numbers, while the New Zealand data from Table 6 are shown as white numbers on a black background. The $\Delta^{14}C$ data are overlaid on profiles of potential vorticity drawn from the GEOSECS data and plotted against the density ordinate.

McCartney [1982] defines the lighter variety of SAMW by a potential density range between 26.80 and 26.95‰, while the heavier variety is defined as a range between 26.95 and 27.10‰. The three southernmost stations in the sequence, 296, 303, and 306, have PV minima which appear to span both types. In Figure 18 the heavier variety of SAMW can be traced as far north as station 263 (17°S) as either a minimum or an inflection point in the PV profiles. The PV minimum associated with the lighter variety of SAMW is not apparent north of station 306 (33°S), presumably due to erosion by mixing. Diapycnal mixing tends to break down the vertical density gradient which defines the top of the PV minimum layer.

TABLE 6.   Subsurface Prebomb $\Delta^{14}C$ Measurements Reported by *Rafter* [1968] Within the Density Range of Subantarctic Mode Water

Sample No.	Latitude °S	Longitude °W	Collection Date	Depth, m	T, °C	GEOSECS Reference Station	S^*	σ_θ^*	$\Delta^{14}C$, ‰
A.407	21.3	177.5	March 1958	580	9	268/520 m	34.54	26.81	-81 ± 6
C.30	29.3	177.3	Sept. 1958	550	10	277/400 m	34.83	26.82	-76 ± 4
C.575	31.8	164.5	Oct. 1960	500	11	306/300 m	34.93	26.73	-54 ± 9

Salinities are not reported for these samples. Temperatures are reported only to the nearest 1°C. We have referenced these samples to the closest GEOSECS station, where the stated tempoerature was used to determine an approximate salinity and density for each sample according to the GEOSECS T, S, and σ_θ profiles. A 1° error in temperature changes σ_θ by ~0.07 units.
*Approximate.

The GEOSECS $\Delta^{14}C$ data points at the base of the PV minimum appear to be uncontaminated with bomb ^{14}C. Five different stations between 45° and 17°S have $\Delta^{14}C$ levels of -86 ± 5‰ at densities close to 27.1, suggesting that there has been no ventilation of this layer over the time scale of the bomb transient. North of 17°S, where all traces of the PV minimum disappear, $\Delta^{14}C$ values make an abrupt jump from -85 to -104‰. *Reid*'s [1965] map of salinity on the 80 cL ton^{-1} steric anomaly surface (at the bottom of the salinity minimum layer) shows the low-salinity signature of this water mass penetrating northward only to about this latitude. Within the dense SAMW proper at a density of 27.0‰ $\Delta^{14}C$ levels average about -57‰. This represents a small amount of bomb contamination but serves as evidence for active ventilation for the denser SAMW layer. In the region of Figure 18 where the lighter variety of SAMW is identifiable, the GEOSECS samples are quite contaminated with bomb ^{14}C. $\Delta^{14}C$ levels from -32 to $+48$‰ characterize the lighter SAMW.

A pair of dashed lines have been drawn across Figure 18 which outline possible water mass trajectories through density-latitude space. The lower dashed line depicts the evolution of the dense variety of SAMW. It has been drawn to connect features observed in the potential vorticity profiles. It stays within one tenth of a σ_θ unit from its initial position at 45°S until it stops where $\Delta^{14}C$ levels jump from -85 to -104‰. The upper dashed line has been drawn as a proposed water mass trajectory for the lighter variety of SAMW. According to the data in Figure 15, 8°C water has a prebomb $\Delta^{14}C$ content between -70 and -85‰. The upper dashed line connects 8°C water at 45°S with the -72‰, 11°C water at 4.5°S. The upward slope of the shallower dashed line represents a substantially larger change in density of about 0.3 σ_θ units.
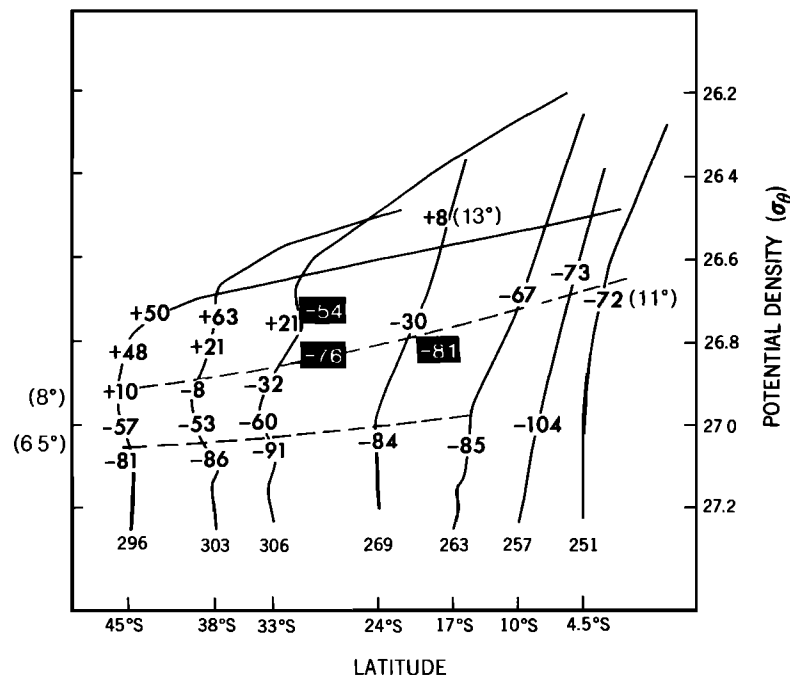
Fig. 18. $\Delta^{14}C$ along the western Pacific transect of GEOSECS stations (Figure 17) plotted as a function of potential density and latitude (plain boldface numbers) (Tables 2 and 5). The GEOSECS data are overlaid on profiles of potential vorticity $(p^{-1}f\partial p/\partial z)$ which are displaced along the x axis to reflect the latitudinal spacing of the stations. Prebomb New Zealand data in Table 6 are shown in white-on-black numbers. The upper and lower dashed curves show the evolution of the lighter and denser varieties of SAMW as the water masses move northward, according to the discussion in the text.

Fig. 19. *T-S* plot showing the evolution of 11°C, −72‰ water in the western Pacific, the Equatorial 13°C Water, and the 15°C water in the Peru-Chile Undercurrent from the lighter variety of Subantarctic Mode Water. To put this *T-S* evolution into context, *T-S* profiles from five GEOSECS stations in the North and South Pacific have been included (for locations see Figure 17). Two of the stations are located in the subsurface low-salinity tongue in the eastern North Pacific (237 and 344), and two are located in 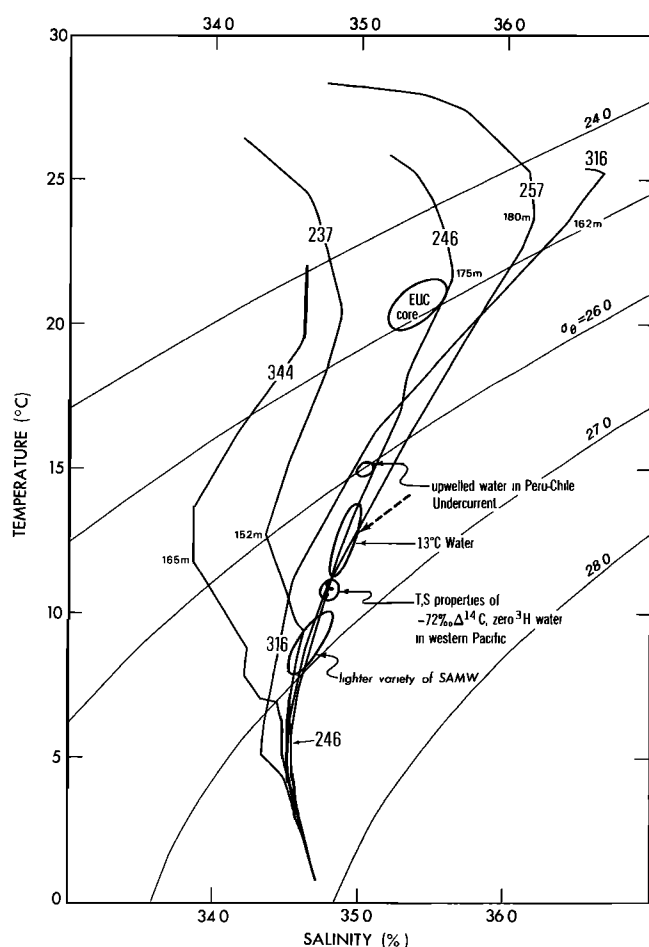the high-salinity tropical underwater in the South Pacific (316 and 257). The constant density evolution of the 13°C Water according to *Tsuchiya* [1981] is shown by the bold dashed arrow following the 26.45 σ_θ contour.

Two of the prebomb New Zealand samples come from water that is just dense enough to be SAMW (~26.81). They have $\Delta^{14}C$ contents of −76 and −81‰. These are important observations. They serve to confirm that prebomb SAMW, or at least remnants of the prebomb SAMW, had nearly the same $\Delta^{14}C$ levels as uncontaminated water in the Equatorial Undercurrent or the prebomb growth bands of the Galapagos coral. The $\Delta^{14}C$ and temperature of these samples fall right on the prebomb $\Delta^{14}C$ versus temperature trend for South Pacific surface water (Figure 15). The third New Zealand data point has roughly the same density and temperature as the −73 and −72‰ data points at the northern end of the GEOSECS transect, but it has a prebomb $\Delta^{14}C$ content of −54‰. This provides further evidence that the tritium-free water in the lower undercurrent did not originate as 11° water or as any water type warmer than 11°C.

In Figure 19 a *T-S* diagram has been constructed from some of the GEOSECS stations identified in Figure 18. We have labeled the regions of *T-S* space which characterize key water masses that figure in the discussion, including the core of the Equatorial Undercurrent, the lighter variety of SAMW, the three water samples containing the −72‰ water in the western equatorial Pacific, the 13°C Water, and the upwelled water from the Peru-Chile Undercurrent. All these water masses plot along a line connecting the Undercurrent core and the lighter variety of SAMW. All the key water masses discussed in this paper can be formed by simple mixing between the lighter variety of SAMW and an upper ocean end-member typified by the warm and salty water found in the subtropical high-salinity water or in the core of the Equatorial Undercurrent.

The constant-density evolution of the 13°C thermostad water according to *Tsuchiya* [1981] is indicated by the dashed arrow along the 26.45‰ isopycnal in Figure 19. Because mixing along the constant density surface with relatively fresh water from the north will act to freshen the thermostad water, Tsuchiya had to find a salty source for the thermostad water. This he found in the surface waters of the southwestern part of the South Pacific subtropical gyre. The SAMW source invoked here is already fresher than the thermostad water. We find a source of salinity to account for the thermostad's *T-S* composition in the warm, salty overlying water. There is little indication from Figure 19 that low-salinity water from the northern hemisphere influences the *T-S* composition of the labeled water masses, except indirectly, perhaps, by freshening the water in the undercurrent core.

SAMW in the GFDL Model

Apart from its prediction regarding the prebomb $\Delta^{14}C$ content of South Pacific surface waters, the *Toggweiler et al.* [1989a, b] model cannot be used to help support the claim that SAMW might be the source of the −72‰ water in the Equatorial Undercurrent. The model does generate a weakly stratified water mass which forms just south of Australia between 40° and 45°S with an initial $\Delta^{14}C$ content of only −45‰. Rather than penetrating the South Pacific thermocline in the western South Pacific like McCartney's mode water, the model's "subaustralian mode water" travels all the way across the Pacific to the coast of South America before moving northward (for more details, see *Toggweiler et al.* [1989b, pp. 8253–8254, 8258–8260, Figure 11].

The model's subaustralian mode water starts off as a well homogenized "mode" of the radiocarbon distribution in Toggweiler et al.'s prebomb simulation. It becomes loaded with bomb ^{14}C in the postbomb simulation and is easily tracked into the South Pacific thermocline and around Drake Passage into the South Atlantic by its bomb ^{14}C buildup. By the year 1990 of the postbomb simulation, the model's subaustralian mode water layer has been well ventilated with bomb-contaminated water up to 15°S. The model does not, however, bring this water mass into the tropics over this time scale.

The Volume of Low-$\Delta^{14}C$ Water Upwelled in the Eastern Equatorial Pacific

The asymmetry in prebomb $\Delta^{14}C$ levels between northern and southern hemisphere surface water provides a way to
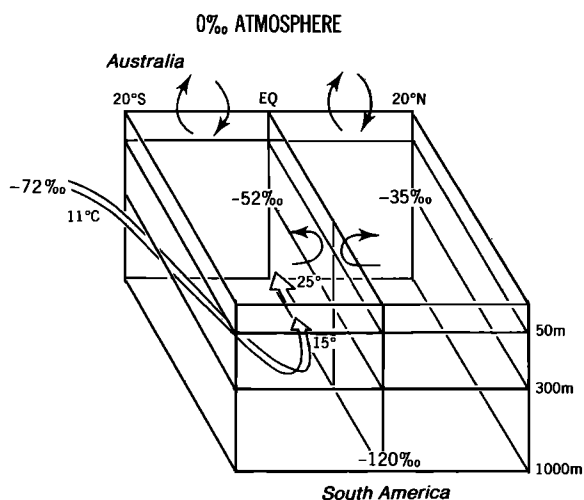
0‰ ATMOSPHERE

Fig. 20. Schematic diagram showing how the flux of low-Δ^{14}C water through the eastern Pacific upwelling system has been calculated. The shallow recirculation through the equatorial upwelling system would be assumed to produce equal Δ^{14}C levels north and south of the equator except that the southern hemisphere has a source of $-72‰$ water that upwells in the east.

compute the volume of low-Δ^{14}C water being upwelled in the tropical South Pacific. Basically, we use knowledge about the rate at which oceanic ^{14}C/^{12}C ratios equilibrate with the atmospheric CO_2 to estimate the dilution effect caused by the input of low-Δ^{14}C water into the tropical South Pacific surface layer. A schematic diagram in Figure 20 illustrates how this calculation is made. If prebomb Δ^{14}C data from Table 1 are simply averaged within each hemisphere, one finds that tropical surface water in the South Pacific is typically 17‰ lower than North Pacific water. If one assumes that the 17‰ difference is due to dilution with upwelled $-72‰$ water in the south, then one can calculate the rate of low-Δ^{14}C water input required to balance the enhanced ^{14}C input from the atmosphere.

We set up a Δ^{14}C balance equation as follows:

$$\frac{g}{Hz} \Delta_{NS} = \frac{w}{z} \Delta_{SD}$$

where g is the gas exchange rate in moles of CO_2 per square meter per year, H is the CO_2 content of typical surface water in moles per cubic meter, z is the thickness of the layer actively exchanging CO_2 with the atmosphere, Δ_{NS} is the prebomb Δ^{14}C difference between the northern and southern hemisphere surface water, w is the basin-average upwelling rate in meters per year, and Δ_{SD} is the prebomb Δ^{14}C difference between the inflowing water and average surface water. We assume that the inflowing low-Δ^{14}C water has a Δ^{14}C of $-72‰$ and typical southern hemisphere surface water has a Δ^{14}C of $-52‰$, such that $\Delta_{SD} = 20‰$. Plugging in the following values, $g = 13$ mol m^{-2}/yr^{-1} [Toggweiler et al., 1989a], $H = 2$ mol/m^{-3}, and $\Delta_{NS} = 17‰$, we compute a value of w equal to 5.5 m yr^{-1}. Given a 50-m mixed layer, this value of w implies that surface waters in the tropical South Pacific are turned over every 10 years or so with lower thermocline water. If we assume the enhanced gas exchange operates over an area defined by the equator, 20°S, 150°E, and 80°W, i.e., 3.2×10^{13} m^2, then the flow of water through

the system required to sustain the larger Δ^{14}C gradient is about 5×10^6 m^3 s^{-1}.

Rotschi [1970] and Magnier et al. [1973] report eastward flows of 11°C water in the lower layers of the undercurrent to be about 4–5 × 10^6 m^3 s^{-1} (Figure 9). Wyrtki [1963] has estimated the removal of water from the Peru-Chile Undercurrent due to coastal upwelling to be about 4×10^6 m^3 s^{-1}. Thus, there is a degree of consistency between the information contained in the asymmetric Δ^{14}C distribution and actual current measurements.

The measured dilution of tropical south Pacific Δ^{14}C levels due to fossil fuel burning in this century (the Suess effect) is very small, only about 2 ± 4‰. In the North Pacific and North Atlantic one typically observes changes of about 10 to 13‰ [Druffel and Linick, 1978; Konishi et al., 1982]. If one combines the equatorward transport of subantarctic water in the thermocline with the poleward transport of its upwelled remnants at the surface, then one has described a large-scale overturning of South Pacific waters which might explain why the oceanic Suess effect is so small in the south. Water upwelling around Antarctica is driven northward and pumped downward into the thermocline by the circumpolar westerlies [Deacon, 1937]. According to the Toggweiler et al. [1989a, b] model, the deep water upwelling south of the ACC only has 2 or 3 years to equilibrate its ^{14}C/^{12}C ratio with atmospheric CO_2 before being pumped down into the thermocline. This is not nearly enough time to allow the subducting water mass to fully incorporate the change in atmospheric Δ^{14}C levels between 1900 and 1950. If surface water in the South Pacific is then turned over every 10 years with lower thermocline water which has not had a full taste of the Suess effect, the smaller Suess effect in the South Pacific begins to make sense.

Continuity in the South Pacific Thermocline

Montgomery and Stroup [1962] and Tsuchiya [1981] have shown that 11°–14° water in the eastern equatorial Pacific is a mode of the equatorial thermocline caused by inflow from the west. Magnier et al. [1973], Taft and Jones [1973], and Tsuchiya et al. [1990] show that 11° water in the western equatorial Pacific is a mode of the Equatorial Undercurrent transport in that sector. McCartney [1982] has shown that 7°–10°C water is a water mass mode of the South Pacific thermocline. Each of these hydrographic features represents an important advective process. Our attempt to reconstruct the prebomb Δ^{14}C distribution using corals and old seawater data reveals that each of these oceanographic features had nearly the same Δ^{14}C content before the bomb tests. The near constancy of prebomb Δ^{14}C levels suggests that each of these features are part of a continuous chain of thermocline features whose end product is the upwelling of undercurrent water to the surface in the eastern equatorial Pacific. The distinctive low-Δ^{14}C signature of these water masses arises from the injection of Antarctic water into the thermocline along the northern edge of the Antarctic Circumpolar Current.

In his discussion of mode water formation, McCartney [1982] points out that mass must be removed from the thermocline layers incorporating SAMW or else the thickness of these layers will grow with time. The upwelling of

low-Δ^{14}C water in the eastern equatorial Pacific would represent a mechanism by which mass associated with the lighter variety of SAMW is removed from the thermocline. This mechanism of thermocline ventilation, if it truly exists, would be unique to the southern hemisphere, because the conditions for forming SAMW are found only along the northern edge of the circumpolar current. The mechanism proposed here might explain why the South Pacific thermocline appears to be so much better ventilated than the North Pacific thermocline with respect to oxygen [*Reid*, 1965].

A test of this hypothesis may be no more difficult than waiting for results of the World Ocean Circulation Experiment (WOCE) Pacific Δ^{14}C results. At the beginning of the GEOSECS era the ocean-atmosphere Δ^{14}C gradient was about 400‰. During the 1990s the ocean-atmosphere Δ^{14}C gradient will be roughly 50 to 70‰, i.e., nearly the same as in prebomb times (40–50‰). To be sure, both oceanic and atmospheric Δ^{14}C levels will remain elevated, but the input of ^{14}C from the atmosphere will again be relatively weak. As the ocean's radiocarbon distribution is resurveyed during the WOCE program, one should begin to see features like those that characterized the prebomb era.

CONCLUSIONS

The Peru upwelling region is well known for its cool, high-nutrient surface water. One expects to see low Δ^{14}C levels in this water. However, the prebomb Δ^{14}C level of −72‰ observed in the Galapagos coral is much lower than expected, given the temperatures observed at the point of upwelling (15°–16°C). Hydrographic observations indicate that the upwelled water off the coast of Peru has its origin in the eastward flow of high-salinity water in the lower layers of the Equatorial Undercurrent. *Tsuchiya* [1981] has suggested that these water masses in the undercurrent have an origin within the subtropical gyre of the South Pacific, but the time scales for ventilation at this level of the thermocline are much too short to account for the prebomb Δ^{14}C observations. According to the analysis presented here, the distinctive low-Δ^{14}C signature of these water masses arises from the injection of low-Δ^{14}C Antarctic water into the thermocline along the northern edge of the Antarctic Circumpolar Current.

Δ^{14}C is a fundamentally different kind of tracer than most oceanographers are used to working with. Because the equilibration time for carbon isotopes in the mixed layer of the ocean is so slow, the prebomb Δ^{14}C level in upwelled water is an unaltered property of the subsurface layers from which the water originates. Because the upper ocean gradients for this tracer are so small, its concentrations in the thermocline should be much less sensitive to the effects of upper ocean mixing than concentrations of other tracers. The radiocarbon data highlighted here suggest that important water masses of the South Pacific, like the lighter variety of Subantarctic Mode Water, the Equatorial 13°C Water, and the Peruvian upwelling all had similar prebomb Δ^{14}C levels (within 10‰). This implies that all may be part of a single advective process of thermocline ventilation, in which each evolves from the one before it by the addition of heat and salt from the warmer and saltier layers above.

The data base on which this analysis is based is quite sparse. Prebomb Δ^{14}C information from the tropics is based on corals and shells from only eight sites. We assume that upwelled water off the coast of Peru had similar Δ^{14}C levels to the prebomb growth bands of the Galapagos coral. Our information from middle and high latitudes is based on a limited set of seawater samples from 1957 and 1958 accompanied by marginal hydrographic information. Given these uncertainties, our conclusion regarding the origin of the upwelled water in the eastern equatorial Pacific should be considered a well-detailed hypothesis rather than an absolute proof. Meanwhile, the effect of atmospheric nuclear testing on upper ocean and atmospheric Δ^{14}C distributions continues to abate. By the mid 1990s the coupling between oceanic and atmospheric Δ^{14}C levels should be nearly restored to prebomb conditions. If this hypothesis is correct, the distinctive features of the tropical and South Pacific prebomb Δ^{14}C distribution should be directly observable before long with modern techniques.

While this analysis makes use of the GFDL ocean circulation model to illustrate general properties of the prebomb radiocarbon field, it is also points out a number of serious problems in the model's circulation field. The model produces its tropical Δ^{14}C minimum via the equatorial divergence. The low-Δ^{14}C subsurface water upwelling at the equator in the model reaches the equator from the north. Both these features are at variance with what hydrographic measurements and prebomb radiocarbon observations suggest. The coarse-resolution model's most clear cut problem stems from a weak Equatorial Undercurrent. This problem is not cause for concern. High-resolution models of the equatorial Pacific [*Philander et al.*, 1987] have no problem generating a vigorous undercurrent. On the other hand, the model's equatorial Pacific Δ^{14}C minimum has its origin in abyssal water upwelling through the thermocline in the eastern North Pacific. The analysis presented here suggests that the low-Δ^{14}C signal comes from Antarctic surface water subducted into the South Pacific thermocline. These represent profoundly different views on how this important deepwater signal reaches the surface in the equatorial Pacific. It is important to know which view is right. It is also important that ocean models get the right answer.

APPENDIX

Table A1 compiles a post-1950 global coral data set for use in model validation exercises. Table A1 includes previously published data from 13 corals and also includes data from 7 corals analyzed at Lamont-Doherty Geological Observatory. Figure A1 shows the locations of coral sites in Table A1. Table A2 gives references and other information about each coral site and data set. We have attempted to place the midpoint of each coral growth year within either the first half or the last half of the calendar year.

Table A3 provides a complete listing of coral ^{14}C measurements produced at LDGO over the last 10 years. Exact locations, collection times, and other pertinent information regarding the LDGO corals appears in Table A2. Some of these results appeared in the first author's Ph.D. thesis [*Toggweiler*, 1983]. Results from the Djibouti coral were published by *Cember* [1989]. Data from the remaining corals have never been published. These measurements were produced by J. White, S. Trumbore, and G. Mathieu.

TABLE A1. Compiled Coral ^{14}C

Year	Tonga (20°S)	Fiji (18°S)	Tahiti (17.5°S)	Abrolhos (18°S)	Cocos (12°S)	Canton (3°S)	Galapagos (1°S)	Tarawa (1°N)	Fanning (4°N)	Ponape (7°N)
1950.0										
1950.5		−68					−70		−58	
1951.0										
1951.5		−65					−75		−61	
1952.0										
1952.5		−52					−69		−55	
1953.0										
1953.5		···			−30		−75		−53	
1954.0										
1954.5		−62			···		−72		−56	
1955.0										
1955.5		−61			···		···		−66	
1956.0										
1956.5		−72			···		···		−64	
1957.0										
1957.5		−46			···		···		−57	
1958.0				−32						
1958.5		−61			···		···		−49	
1959.0				···						
1959.5		−37			···		···		−39	
1960.0				···				−34		
1960.5	−26	−27			···		···		−47	
1961.0				···				−45		
1961.5	−48	···			···		−59		−29	
1962.0				···				−38		
1962.5	−74	···			···		−51		−33	
1963.0				···				−13		
1963.5	−35	3			···		−44		−2	
1964.0				···				7		
1964.5	−24	34			···		−24		6	
1965.0				50				49		
1965.5	3	56			···		−5		22	
1966.0				···				37		
1966.5	···	58			···		−25		32	
1967.0				85				40		
1967.5	3	90			···		+1		39	
1968.0				···				48		
1968.5	48	102			···	40	15		50	
1969.0			99	···		59		59		
1969.5	···	90			···	48	31		64	
1970.0				···		56		62		
1970.5	86	115	113		118	59	20.5		58	
1971.0				140		57		57		
1971.5	···	122			···	66	28		69	
1972.0			118	···		73		91		
1972.5	108	125	128		129	69	39		85	105
1973.0			128	···		80		85		
1973.5	114	135	136	139	130	77	22.5		71	···
1974.0			136	···				89		
1974.5	···	138			134		27		80	118
1975.0				149				97		
1975.5	157	133			···		39		···	···
1976.0								82		
1976.5	142	121			121		47		···	···
1977.0								88		
1977.5	146	115					63		96	···
1978.0								91		
1978.5		104					24		108	129
1979.0								103		
1979.5							54		100	···
1980.0										
1980.5							38			131
1981.0										
1981.5							46			
1982.0										
1982.5							80			
1983.0										
1983.5										
1984.0										
1984.5										

Dots indicate that coral material exists for given years and could still be analyzed. Blanks represent years that either predate the growth

Data for the Postbomb Era

Panama (8°N)	Djibouti (12°N)	Belize (17°N)	Oahu A (21°N)	Oahu B (21°N)	French Frigate Shoals (24°N)	Okinawa (26.5°N)	Florida Keys (25°N)	Bermuda A (32°N)	Bermuda B (32°N)
		−54				−36	−53		
−64	−73	···				···	−65	−52	−46.0
	···	−66				−42	−66		−54.8
−58	···	···				−43	−58		−47.8
	···	···				−41	−55	−58	···
−51	···	−54				−36	−60		···
−46	···	···				+2	−54.4		···
−47	···	−40				−15	−54	−33	−46.6
−45	−61	−44.5	−61		−23	−12	−48.6		−44.9
−37	−57	−20	−49		···	−12	−28		−41.8
−42	−52	−18			···	−2	−18.0	−34	−26.8
−24	−46	−12	−13		···	−1	−12		−18.7
−26	−30	26	5		14	6	3.4		−5.6
−22	−13	28	31		68	35	45	−12	−2.1
23	−7	71	···		84	60	71.8		25.8
29	9	98	71		118	···	108		62.3
46	···	127	75		114	102	120.0	74	79.6
34	37	131	126		159	···	140		95.8
66	23	140	126		173	134	143		110.5
74	39	131	168		164	···	146	96	116.8
70	45	154	153	131	177	167	156		127.8
···	45	142	160	161	189	168	152		138.0
75	51	156	174	156	182	175	155	82	145.6
67	50	149	···	166	188	176	148.5		153.6
70	50	149	175	159	177	···	150.0		157.6
56	44	149	156	161	179	179	154	167	146.5
43	46	152	155	157	168	176	135		150.7
54	41	155	134	139	164	177	134		150.8
52	43		136	127	165	···	132.5		158.8
74	52		143	132		170	135.3		154.9
73	44					160	128.3		146.3
	47						127.2		144.8
	46						128.3		148.7
	50						115.3		140.1
	50								127.9

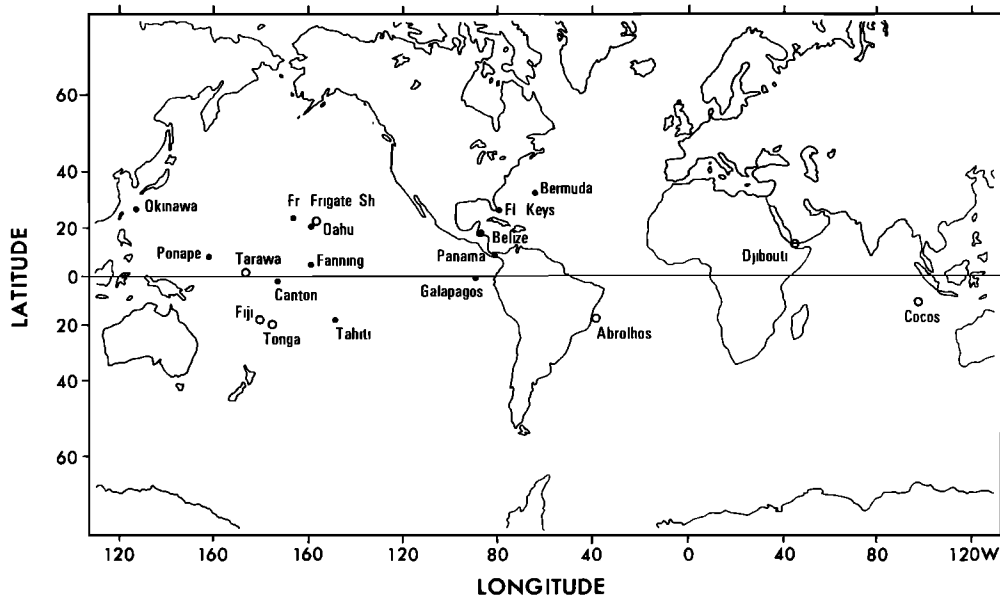of the coral or occur after its collection.

Fig. A1. Locations of coral sites in Tables A1, A2, and A3. Open circles denote corals analyzed at LDGO. Complete data from these sites are compiled in Table A3. Solid circles denote corals analyzed elsewhere. Annual post-1950 data from all sites are compiled in Table A1.

TABLE A2. References and Notes for Coral Sites Listed in Table A1

Site	Notes
Tonga (S. Pacific, 20°S, 175°W)	Collected April 1979 by R. Fairbanks. Data reported in Table A3. Errors average 9‰. Midpoint of growth band estimated to be midyear.
Fiji (S. Pacific, 18°S, 179°E)	Collected April 1979 by R. Fairbanks. Data reported by Toggweiler [1983] and in Table A3. Errors average 6‰. Midpoint of growth bands estimated to be midyear.
Tahiti (S. Pacific, 17°29'S, 149°36'W)	Collected March 1974. Data reported by Druffel [1987]. Errors reported to be 3–4‰. Coral reported to accrete 5 bands/year. Detailed chronology given by author.
Abrolhos Banks (Brazil, 18°S, 39°W)	Collected January 1983 by S. Trumbore. Data reported in Table A3. Errors average 9‰. Midpoint of growth band estimated to be at beginning/end of year.
Cocos–Keeling Island (Indian Ocean, 12°S, 97°E)	Collected April 1978 by J. R. Toggweiler. Data reported in Table A3. Errors ~8‰. Midpoint of growth bands estimated to be midyear.
Canton Island (equatorial Pacific, 2°48'S, 171°43'W)	Collected September 1973. Data reported by Druffel [1987]. Errors 3–4‰. Coral was sectioned into semiannual bands with midpoints at ~May–June and November–December.
Galapagos (equatorial Pacific, 1°S, 90°W)	Record comes from several coral heads collected in February 1976 and 1982. Data reported by Druffel [1981, 1987]. Errors 3–4‰. Midpoint of growth bands reported to be midyear. For 1973–1976, data from Hood and Santa Cruz islands have been averaged.
Tarawa (equatorial Pacific, 1°N, 172°E)	Collected April 1979 by R. Fairbanks. Data reported by Toggweiler [1983] and in Table A3. Errors average 8‰. Midpoint of growth bands estimated to be early fall.
Fanning Island (equatorial Pacific, 3°52'N, 159°23'W)	Collected April 1979 by J. R. Toggweiler. Radiocarbon analyses by E. Druffel. Data reported by Druffel [1987]. Errors 3–4‰. Midpoint of growth band estimated to be midyear.
Ponape Island (equatorial Pacific, 7°00'N, 158°12'E)	Collected 1980. Data given in graphical form by Konishi et al. [1982]. No estimate of growth year given. We assume midpoints of growth bands represent midyear. Error 5–6‰.
Uva Island (Panama (Pacific side), 7°48'N, 81°45'W)	Collected July 1980. Data reported by Druffel [1987]. Midpoint of growth band assumed to be midyear. Errors 3–4‰.
Djibouti (Gulf of Aden, 12°N, 43°E)	Collected January 1985 by R. Cember. Data reported by Cember [1989] and in Table A3. Errors ~8‰. Midpoint of growth band reported to be late summer–early fall.
Belize (Caribbean Sea, 16°50'N, 87°48'W)	Collected July 1977 by J. H. Hudson and E. A. Shinn. Data reported by Druffel [1980]. Errors 3–4‰. Midpoint of growth band reported to be late winter–early spring.
Oahu A (Hawaiian Islands, N. Pacific, 21°N, 158°W)	Collected May 1979 by R. Fairbanks. Data reported by Toggweiler [1983] and in Table A3. Errors 6–7‰. Banding in this coral reported to be irregular; chronology determined by $\delta^{18}O$ [Toggweiler and Trumbore, 1985].
Oahu B (Hawaiian Islands, N. Pacific, 21°18'N, 158°07'W)	Collected October 1978. Data reported by Druffel [1987]. Errors 3–4‰. Midpoint of growth band assumed to be late winter–early spring.
French Frigate Shoals (Hawaiian Islands, N. Pacific, 23°43'N, 166°06'W)	Collected November 1978. Data reported by Druffel [1987]. Errors 3–4‰. Midpoint of growth band assumed to be late winter–early spring.
Okinawa (N. Pacific, 26°N, 128°E)	Collected 1980. Data given in graphical form by Konishi et al. [1982]. No estimate of growth year given. We assume midpoint of growth year in late winter following pattern of other north temperate corals. Errors 5–6‰.
Florida Keys (N. Atlantic, 24°57'W, 80°33°W)	Samples collected from cores of large coral heads taken in June 1975, July 1978, and 1983 by J. H. Hudson and E. Druffel. Data reported by Druffel and Linick [1978] and Druffel [1980, 1989]. Errors for early work in range 4–8‰; errors for more recent work reported to be 2.5‰. Approximately half the yearly values reported here represent error-weighted averages. Midpoint of growth band reported to be late winter.
Bermuda A (N. Atlantic, 32°N, 65°W)	Collected July 1976. Data reported by Nozaki et al. [1978]. Errors ~10‰. Bomb ^{14}C reported for samples representing three annual bands.
Bermuda B (N. Atlantic, 32°N, 65°W)	Collected 1983. Data reported by Druffel [1989]. Errors ~2.5‰. Midpoint of growth year reported to be early fall.

TABLE A3. Tabulated LDGO Coral ^{14}C Data

Sample No.	Midpoint Growth Year	Δ^{14}C, ‰
	*Tarawa**	
1537A	1959.8	−34.3 ± 7.8
1537B	1960.8	−44.6 ± 7.1
1537C	1961.8	−37.7 ± 7.1
1537D	1962.8	−12.7 ± 7.1
1537E	1963.8	6.9 ± 6.4
1537F	1964.8	48.8 ± 10.4
1537G	1965.8	37.1 ± 8.0
1537H	1966.8	40.0 ± 6.9
1937I	1967.8	47.9 ± 8.2
1537J	1968.8	59.0 ± 7.3
1537K	1969.8	62.2 ± 7.8
1537L	1970.8	56.5 ± 8.6
1537M	1971.8	90.5 ± 11.2
1537N	1972.8	85.0 ± 7.0
1537O	1973.8	89.3 ± 9.2
1537P	1974.8	96.7 ± 6.4
1537Q	1975.8	82.1 ± 8.6
1537R	1976.8	88.1 ± 8.8
1537S	1977.8	91.1 ± 7.8
1537T	1978.8	103.0 ± 7.2
	*Oahu**	
1559A	1958.0	−61.0 ± 8.1
1559B	1959.0	−49.0 ± 11.0
1559C	1960.5	−12.7 ± 6.8
1559D	1961.7	4.8 ± 5.7
1559E	1962.8	31.4 ± 5.9
1559F	1964.4	71.2 ± 7.5
1559G	1965.8	75.0 ± 7.9
1559H	1966.8	125.8 ± 6.5
1559I	1968.0	126.4 ± 5.4
1559J	1968.6	167.6 ± 6.6
1559K	1969.5	153.0 ± 6.5
1559L	1970.7	160.3 ± 6.4
1559M	1971.7	174.2 ± 8.1
1559O	1973.4	174.5 ± 6.7
1559P	1974.2	156.3 ± 6.8
1559R	1976.1	155.1 ± 8.0
1559S	1976.8	156.1 ± 6.6
1559T	1977.7	134.4 ± 13.0
1559U	1978.4	135.9 ± 8.0
1559V	1979.1	142.9 ± 6.6
	*Fiji**	
1561A	1930	−44.3 ± 6.0
1561B	1938–40	−55.7 ± 5.0
1561C	1949.5	−57.4 ± 5.4
1561D	1950.5	−70.0 ± 5.3
1561E	1951.5	−65.2 ± 5.2
1561F	1952.5	−51.9 ± 6.2
1561H	1954.5	−57.0 ± 5.4
1561I	1955.5	−60.9 ± 5.2
1561J	1956.5	−71.7 ± 5.2
1561K	1957.5	−45.7 ± 5.0
1561M	1959.5	−37.0 ± 6.0
1561N	1960.5	−27.0 ± 5.7
1561Q	1963.5	2.6 ± 5.5
1561R	1964.5	33.8 ± 5.2
1561S	1965.5	56.2 ± 5.9
1561T	1966.5	58.2 ± 6.6
1561U	1967.5	89.9 ± 6.1
1561W	1969.5	89.8 ± 6.4
1561X	1970.5	115.3 ± 5.8
1561Y	1971.5	121.5 ± 5.8
1561Z	1972.5	124.7 ± 6.5
1561DD	1976.5	120.9 ± 5.6
1577D	1925.5	−83.4 ± 9.4
1577R	1939.5	−54.4 ± 5.7
1577S	1940.5	−53.2 ± 5.2
1577T	1941.5	−56.5 ± 5.0
1577U	1942.5	−61.8 ± 7.8

TABLE A3. (continued)

Sample No.	Midpoint Growth Year	Δ^{14}C, ‰
	Fiji (continued)	
1577V	1943.5	−66.8 ± 6.0
1577W	1944.5	−63.7 ± 5.5
1577Z	1947.5	−62.0 ± 5.9
1577AA	1948.5	−66.4 ± 4.7
1577CC	1950.5	−65.3 ± 9.6
1577GG	1954.5	−66.7 ± 6.1
1577KK	1958.5	−60.9 ± 6.5
1577UU	1968.5	101.8 ± 7.1
1577ZZ	1973.5	134.8 ± 7.4
1577AAA	1974.5	138.0 ± 6.9
1577BBB	1975.5	132.8 ± 6.3
1577DDD	1977.5	115.1 ± 7.6
1577EEE	1978.5	104.0 ± 10.6
	Cocos	
1657	1941	−78.0 ± 8.2
1583A	1953.5	−29.5 ± 9
1583R	1970.5	117.9 ± 9
1583T	1972.5	128.5 ± 9
1583U	1973.5	130.0 ± 8.3
1583V	1974.5	134.1 ± 8.2
1583X	1976.5	121.3 ± 8.4
	Tonga	
1587A	1960.5	−26.2 ± 10.5
1587B	1961.5	−47.5 ± 9.1
1587C	1962.5	−73.9 ± 8.8
1587D	1963.5	−34.7 ± 10.0
1587E	1964.5	−23.9 ± 9.0
1587F	1965.5	2.8 ± 9.1
1587H	1967.5	3.1 ± 9.5
1587I	1968.5	47.9 ± 8.7
1587K	1970.5	85.7 ± 8.4
1587M	1972.5	108.0 ± 8.7
1587N	1973.5	114.2 ± 10.7
1587P	1975.5	156.5 ± 9.1
1587Q	1976.5	141.5 ± 9.3
1587R	1977.5	146.4 ± 9.0
	Abrolhos Banks	
1614G	1958.0	−32.3 ± 9.1
1614K	1965.0	50.2 ± 12.4
1614L	1967.0	84.7 ± 9.2
1614O	1971.0	139.8 ± 8.7
1614P	1973.5	139.3 ± 8.1
1614Y+Z	1975.0	148.8 ± 7.7
	Mauritius	
1615F	1972.5	201.2 ± 13.0
1615I	1975.5	142.2 ± 9.4
1615K	1977.7	161.4 ± 9.6
	Djibouti†	
1659	1951.0	−73.4 ± 8.5
1650B	1958.8	−61.2 ± 7.8
1650C	1959.8	−57.2 ± 7.8
1650D	1960.8	−51.5 ± 8.8
1650E	1961.8	−46.0 ± 7.7
1650F	1962.8	−29.5 ± 8.0
1650G	1963.8	−12.9 ± 8.6
1650H	1964.8	−6.9 ± 8.8
1650I	1965.8	9.4 ± 7.6
1650K	1967.8	37.0 ± 7.8
1650L	1968.8	22.5 ± 8.0
1650M	1969.8	39.3 ± 9.2
1650N	1970.8	44.6 ± 7.6
1650O	1971.8	44.9 ± 7.9
1650P	1972.8	50.6 ± 7.9
1650Q	1973.8	50.1 ± 7.4
1650R	1974.8	49.9 ± 9.0
1650S	1975.8	44.0 ± 7.5
1650T	1976.8	46.2 ± 7.9

TABLE A3. (continued)

Sample No.	Midpoint Growth Year	$\Delta^{14}C$, ‰
	Djibouti† (continued)	
1650U	1977.8	41.0 ± 7.6
1650V	1978.8	42.5 ± 7.5
1650W	1979.8	51.5 ± 7.4
1650X	1980.8	44.2 ± 7.6
1650Y	1981.8	46.6 ± 7.5
1650Z	1982.8	45.6 ± 7.4
1650AA	1983.8	50.3 ± 8.4
1650BB	1984.8	49.6 ± 7.5

*Data from Tarawa, Oahu, and 1561 series Fiji corals are given by *Toggweiler* [1983].

†Data from Djibouti are given by *Cember* [1989].

REFERENCES

Bien, G. S., N. W. Rakestraw, and H. E. Suess, Radiocarbon in the Pacific and Indian oceans and its relation to deep water movements, *Limnol. Oceanogr., 10*, suppl., R25–R37, 1965.

Brockmann, C., E. Fahrbach, A. Huyer, and R. L. Smith, The poleward undercurrent along the Peru Coast: 5–15°S, *Deep Sea Res., 27*, 847–856, 1980.

Broecker, W. S., and E. A. Olson, Lamont radiocarbon measurements VIII, *Radiocarbon, 3*, 176–204, 1961.

Broecker, W. S., and T.-H. Peng, Gas exchange rates between air and sea, *Tellus, 26*, 21–35, 1974.

Broecker, W. S., and T.-H. Peng, *Tracers in the Sea*, 690 pp., Lamont-Doherty Geological Observatory, Palisades, N. Y., 1982.

Broecker, W. S., D. W. Spencer, and H. Craig, *GEOSECS Pacific Expedition*, vol. 3, Hydrographic Data, U.S. Government Printing Office, Washington, D. C., 1982.

Broecker, W. S., T.-H. Peng, H. G. Ostlund, and M. Stuiver, The distribution of bomb radiocarbon in the ocean, *J. Geophys. Res., 90*, 6953–6970, 1985.

Bryan, K., and L. J. Lewis, A water mass model of the world ocean circulation, *J. Geophys. Res., 84*, 2503–2517, 1979.

Bryden, H. L., and E. C. Brady, Diagnostic model of the three-dimensional circulation in the upper equatorial Pacific Ocean, *J. Phys. Oceanogr., 15*, 1255–1273, 1985.

Cember, R. P., Bomb radiocarbon in the Red Sea: a medium scale gas exchange experiment, *J. Geophys. Res., 94*, 2111–2123, 1989.

Chavez, F. P., and R. T. Barber, An estimate of new production in the equatorial Pacific, *Deep Sea Res., 34*, 1229–1243, 1987.

Colgan, M. W., and D. L. Malmquist, The Urvina Bay uplift: A dry trek through a Galapagos coral reef, *Oceanus, 30*, 61–66, 1987.

Deacon, G. E. R., The hydrology of the southern ocean, *Discovery Rep., 15*, 1–124, plates I–XLIV, 1937.

Druffel, E. R. M., Radiocarbon in annual coral rings of the Pacific and Atlantic oceans, Ph.D. thesis, 213 pp., Univ. of Calif., San Diego, 1980.

Druffel, E. R. M., Radiocarbon in annual coral rings from the eastern tropical Pacific Ocean, *Geophys. Res. Lett., 8*, 59–62, 1981.

Druffel, E. R. M., Bomb radiocarbon in the Pacific: Annual and seasonal timescale variations, *J. Mar. Res., 45*, 667–698, 1987.

Druffel, E. R. M., Variability of ventilation in the North Atlantic determined from high precision measurements of bomb radiocarbon in banded corals, *J. Geophys. Res., 94*, 3271–3285, 1989.

Druffel, E. R. M., and T. W. Linick, Radiocarbon in annual coral rings of Florida, *Geophys. Res. Lett., 5*, 913–916, 1978.

Druffel, E. R. M., and H. E. Suess, On the radiocarbon record in banded corals: Exchange parameters and net transport of $^{14}CO_2$ between atmosphere and surface ocean, *J. Geophys. Res., 88*, 1271–1280, 1983.

Fine, R. A., W. H. Peterson, and H. G. Ostlund, The penetration of tritium into the tropical Pacific, *J. Phys. Oceanogr., 17*, 553–564, 1987.

Gillespie, R., and H. A. Pollach, The suitability of marine shells for radiocarbon dating of Australian prehistory, in *Radiocarbon Dating*, edited by R. Berger and H. E. Suess, pp. 404–421, University of California Press, Berkeley, 1979.

Keeling, C. D., Carbon dioxide in surface ocean waters, 4, Global distribution, *J. Geophys. Res., 73*, 4543–4553, 1968.

Knutson, D. W., R. W. Buddemeier, and S. V. Smith, Coral chronometers: Seasonal growth bands in reef corals, *Science, 177*, 270–272, 1972.

Konishi, K., T. Tanaka, and M. Sakanoue, Secular variation of radiocarbon concentration in sea water: Sclerochronological approach, in *Proceedings of the Fourth International Coral Reef Symposium*, vol. 1, edited by E. D. Gomez, pp. 181–185, Marine Science Center, University of the Philippines, Manila, 1982.

Jenkins, W. J., ^3H and ^3He in the Beta Triangle: Observations of gyre ventilation and oxygen utilization rates, *J. Phys. Oceanogr., 17*, 763–783, 1987.

Levitus, S., Climatological atlas of the world ocean, *NOAA Prof. Pap. 13*, 173 pp., U.S. Govt. Print. Off., Washington, D. C., 1982.

Lindstrom, E., R. Lukas, R. Fine, E. Firing, S. Godfrey, G. Meyers, and M. Tsuchiya, The Western Equatorial Pacific Ocean Circulation Study, *Nature, 330*, 533–537, 1987.

Lukas, R., The termination of the Equatorial Undercurrent in the Eastern Pacific, *Prog. Oceanogr., 16*, 63–90, 1986.

Magnier, Y., H. Rotschi, P. Rual, and C. Colin, Equatorial circulation in the western Pacific (170°E), *Prog. Oceanogr., 6*, 29–46, 1973.

McCartney, M. S., Subantarctic mode water, in *A Voyage of Discovery*, edited by M. Angel, pp. 103–119, Pergamon, Elmsford, N. Y., 1977.

McCartney, M. S., The subtropical recirculation of mode waters, *J. Mar. Res., 40*, suppl., 427–464, 1982.

Montgomery, R. B., and E. D. Stroup, Equatorial waters and currents at 150°W in July–August 1952, *Johns Hopkins Oceanogr. Stud., 1*, 68 pp., 1962.

Murphy, P. P., R. A. Feely, R. H. Gammon, D. E. Harrison, K. C. Kelly, and L. S. Waterman, Assessment of the air-sea exchange of CO_2 in the South Pacific during austral summer, *J. Geophys. Res.*, this issue.

Murray, J. M., J. N. Downs, S. Strom, C.-L. Wei, and H. Jannasch, Nutrient assimilation, export production, and ^{234}Th scavenging in the eastern equatorial Pacific, *Deep Sea Res., 36*, 1471–1489, 1989.

Nozaki, Y., D. M. Rye, K. K. Turekian, and R. E. Dodge, A 200-year record of carbon-13 and carbon-14 variations in Bermuda coral, *Geophys. Res. Lett., 5*, 825–828, 1978.

Oort, A. H., Global atmospheric circulation statistics 1958–1973, 180 pp., *NOAA Prof. Pap. 14*, U.S. Government Printing Office, Washington, D. C., 1983.

Ostlund, H. G., H. Craig, W. S. Broecker, and D. Spencer, *GEOSECS Atlantic, Pacific, and Indian Ocean Expeditions*, vol. 7, Shorebased Data and Graphics, U.S. Government Printing Office, Washington, D. C., 1987.

Philander, S. G. H., and W. J. Hurlin, The heat budget of the tropical Pacific Ocean in a simulation of the 1982–83 El Niño, *J. Phys. Oceanogr., 18*, 926–931, 1988.

Philander, S. G. H., W. J. Hurlin, and A. D. Seigel, Simulation of the seasonal cycle of the tropical Pacific Ocean, *J. Phys. Oceanogr., 17*, 1986–2002, 1987.

Quay, P. D., M. Stuiver, and W. S. Broecker, Upwelling rates for the equatorial Pacific Ocean derived from the bomb ^{14}C distribution, *J. Mar. Res., 41*, 769–792, 1983.

Quinn, W. H., Monitoring and predicting El Niño invasions, *J. Appl. Meteorol., 13*, 825–830, 1974.

Rafter, T. A., Carbon-14 variations in nature, 3, ^{14}C measurements

in the South Pacific and Antarctic oceans, *N. Z. J. Sci.*, *11*, 551–589, 1968.

Reid, J. L., *Intermediate Waters of the Pacific Ocean*, 85 pp., Johns Hopkins Press, Baltimore, Md., 1965.

Reid, J. L., Sea-surface temperature, salinity, and density of the Pacific Ocean in summer and winter, *Deep Sea Res.*, *16*, suppl., 215–224, 1969.

Robinson, G. R., Negative effects of the 1982–83 El Niño on Galapagos marine life, *Oceanus*, *30*, 42–48, 1987.

Robinson, M. K., Atlas of North Pacific Ocean monthly mean temperatures and mean salinities of the surface layer, *Ref. Publ. 2*, Nav. Oceanogr. Off., Suitland, Md., 1976.

Rotschi, H., Variations of equatorial currents, in *Scientific Exploration of the South Pacific*, edited by W. S. Wooster, pp. 75–83, National Academy of Sciences, Washington, D. C., 1970.

Stuiver, M., and P. D. Quay, Atmospheric ^{14}C changes resulting from fossil fuel CO_2 release and cosmic ray flux variability, *Earth Planet. Sci. Lett.*, *53*, 349–362, 1981.

Suess, H. E., Radiocarbon concentration in modern wood, *Science*, *122*, 415, 1955.

Taft, B. A., and J. H. Jones, Measurements of the Equatorial Undercurrent in the eastern Pacific, *Prog. Oceanogr.*, *6*, 47–110, 1973.

Toggweiler, J. R., A six zone regionalized model for bomb radiotracers and CO_2 in the upper kilometer of the Pacific Ocean, Ph.D. thesis, Columbia Univ., New York, 1983.

Toggweiler, J. R., and S. Trumbore, Bomb-test ^{90}Sr in Pacific and Indian Ocean surface water as recorded by banded corals, *Earth Planet. Sci. Lett.*, *74*, 306–314, 1985.

Toggweiler, J. R., K. Dixon, and K. Bryan, Simulations of radiocarbon in a coarse-resolution world ocean model, 1, Steady state prebomb distributions, *J. Geophys. Res.*, *94*, 8217–8242, 1989a.

Toggweiler, J. R., K. Dixon, and K. Bryan, Simulations of radiocarbon in a coarse-resolution world ocean model, 2, Distributions of bomb-produced carbon 14, *J. Geophys. Res.*, *94*, 8243–8264, 1989b.

Tsuchiya, M., *Upper Waters of the Intertropical Pacific Ocean*, 50 pp., Johns Hopkins Press, Baltimore, Md., 1968.

Tsuchiya, M., The origin of the Pacific Equatorial 13°C Water, *J. Phys. Oceanogr.*, *11*, 794–812, 1981.

Tsuchiya, M., R. Lukas, R. A. Fine, E. Firing, and E. Lindstrom, Source waters of the Pacific Equatorial Undercurrent, *Prog. Oceanogr.*, *23*, 101–147, 1990.

Wooster, W. S., and M. Gilmartin, The Peru-Chile Undercurrent, *J. Mar. Res.*, *19*, 97–122, 1961.

Wyrtki, K., The horizontal and vertical field of motion in the Peru Current, *Bull. Scripps Inst. Oceanogr.*, *8*, 313–346, 1963.

Wyrtki, K., Oceanography of the eastern equatorial Pacific Ocean, *Oceanogr. Mar. Biol.*, *4*, 33–68, 1966.

Wyrtki, K., El Niño—The dynamic response of the equatorial Pacific Ocean to atmospheric forcing, *J. Phys. Oceanogr.*, *5*, 572–584, 1975.

Wyrtki, K., An estimate of equatorial upwelling in the Pacific, *J. Phys. Oceanogr.*, *11*, 1205–1214, 1981.

Wyrtki, K., E. Stroup, W. Patzert, R. Williams, and W. Quinn, Predicting and observing El Niño, *Science*, *191*, 343–346, 1976.

Wyrtki, K., E. Firing, D. Halpern, R. Knox, G. J. McNally, W. C. Patzert, E. D. Stroup, B. A. Taft, and R. Williams, The Hawaii to Tahiti Shuttle Experiment, *Science*, *211*, 22–28, 1981.

W. S. Broecker, Lamont-Doherty Geological Observatory of Columbia University, Palisades, NY 10964.

K. Dixon and J. R. Toggweiler, NOAA Geophysical Fluid Dynamics Laboratory, Princeton University, P.O. Box 308, Princeton, NJ 08542.